Review Article

Jinmei Chen, Xiaosong Jiang*, Hongliang Sun, Zhenyi Shao, Yongjian Fang, and Rui Shu

# Phase transformation and strengthening mechanisms of nanostructured high-entropy alloys

https://doi.org/10.1515/ntrev-2021-0071
received August 2, 2021; accepted August 20, 2021

**Abstract:** High-entropy alloys (HEAs) have become a research focus because of their easy access to nanostructures and the characteristics of high strength, hardness, wear resistance, and oxidation resistance, and have been applied in aerospace lightweight materials, ultrahigh temperature materials, high-performance materials, and biomimetic materials. At present, the study of HEAs mainly focuses on the microstructure and mechanical properties. HEAs of Mo, Ti, V, Nb, Hf, Ta, Cr, and W series have high strength, while HEAs of Fe, Co, Ni, Cr, Cu, and Mn series have good toughness. However, the emergence of medium-entropy alloys, metastable HEAs, dual-phase HEAs, and multiphase HEAs increased the complexity of the HEA system, and the phase transition mechanism and strengthening and toughening mechanisms were not fully established. In this article, the preparation, phase formation, phase transformation as well as strengthening and toughening mechanisms of the HEAs are reviewed. The inductive effects of alloying elements, temperature, magnetism, and pressure on the phase transformation were systematically analyzed. The strengthening mechanisms of HEAs are discussed, which provides a reference for the design and performance optimization of HEAs.

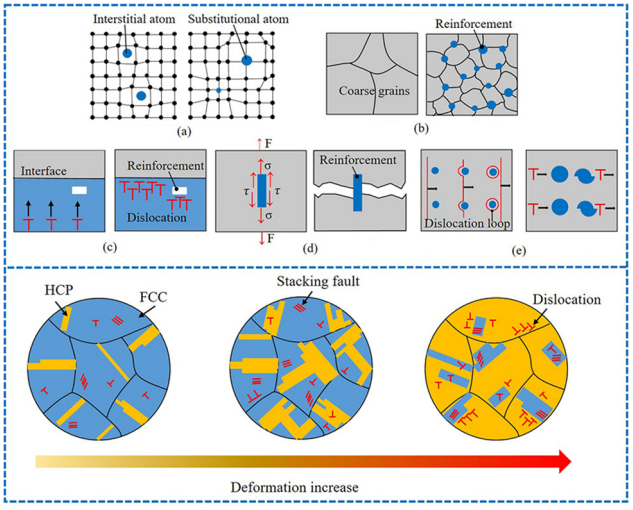


Graphical abstract

**Keywords:** high-entropy alloys, phase transformation, strengthening mechanisms

## 1 Introduction

In the early stage of the development of high-entropy alloys (HEAs), the concept was that five or more elements were alloyed according to equiatomic ratio to form a single-phase solid solution [1–3]. Due to the hysteretic diffusion effect on the dynamics of HEAs, the nucleation and growth rate are limited, and the nanostructure is easily obtained. In general, HEAs with face-centered cubic (FCC) structure have good toughness but are relatively soft [4,5], while HEAs with body-centered cubic (BCC) structure have higher hardness but are relatively brittle [6,7]. FCC-$Fe_{40}Mn_{40}Co_{10}Cr_{10}$ has high ductility (74%) [4]. BCC-$TiNbTa_{0.5}ZrAl_{0.5}$ has the yield strength of 1,740 MPa with ductility of 12% [8]. Therefore, the

* **Corresponding author: Xiaosong Jiang,** Key Laboratory of Advanced Technologies of Materials, Ministry of Education, Chengdu 610031, China; Department of Metal Materials, School of Materials Science and Engineering, Southwest Jiaotong University, Chengdu Sichuan 610031, China, e-mail: xsjiang@swjtu.edu.cn, tel: +86-28-87634177, fax: +86-28-87634177
**Jinmei Chen, Hongliang Sun, Zhenyi Shao:** Key Laboratory of Advanced Technologies of Materials, Ministry of Education, Chengdu 610031, China; Department of Metal Materials, School of Materials Science and Engineering, Southwest Jiaotong University, Chengdu Sichuan 610031, China
**Yongjian Fang:** Department of Mechanical Engineering, Sungkyunkwan University, 2066 Seobu-ro, Jangan-gu, Suwon-si, Gyeonggi-do, 16419, Republic of Korea
**Rui Shu:** Forschungszentrum Jülich GmbHInstitut für Energie-und Klimaforschung Plasmaphysik (IEK-4), 52425 Jülich, Germany

type of crystal structure is an important factor to control the strength, hardness, and plasticity of HEAs. The crystal structure of the HEAs is closely related to the thermodynamic parameters [9,10]. The phase formation criterion related to the thermodynamic parameters plays a guiding role in the design of HEAs.

However, the emergence of medium-entropy alloys [11], metastable HEAs [12,13], and multiphase HEAs [6] broke the original definition to find more interesting properties. HEAs with near equiatomic ratio are often accompanied by brittle intermetallic compounds, such as NiAl-type B2 [14] and complex σ phases [15], and reduce the ductile nanoparticles, such as nano-$L1_2$, which require the high value of Ni/Al [12,16]. Yang *et al.* [17] prepared the $Ni_{30}Co_{30}Fe_{13}Cr_{15}Al_6Ti_6$ HEA with non-equal atomic ratio reinforced by $L1_2$ nanoparticles, and the yield strength is 925 MPa, and the tensile elongation is 43%.

Moreover, metastable HEAs provide a new idea for the optimization of mechanical properties. By reducing the phase stability and promoting phase transformation induced plastic (TRIP) deformation effect, the synergistic strength and toughness of HEAs can be achieved [18–21], mainly including the transformation between BCC and FCC [22,23] and from FCC to close-packed hexagonal (HCP) [24,25]. Cheng *et al.* [18] selected the critical composition of $Al_x$CoCrFeNi in FCC and BCC to reduce the stability of BCC and induce phase transformation by pressure, while Nene *et al.* [20] added Si in $Fe_{42}Mn_{28}Co_{10}Cr_{15}$ to reduce the phase stability. However, the influencing factors of the phase transition of HEAs are very disorderly, and the relationship between these factors and the microstructure has not been established.

In order to optimize the mechanical properties of HEAs, many effective methods have been proposed, such as composition control [22,23], adding reinforcements [26,27], twin induced plastic (TWIP) deformation effect [28,29] and TRIP effect [20,21]. Sathiyamoorthi *et al.* [30] summarized the relationship between the strength and toughness synergy and the microstructure of HEAs with heterogeneous microstructures in a recent review. However, the characteristics of multicomponent, system independence, and continuous evolution of definition increase the degree of freedom of HEAs. In this large and chaotic system, the strengthening and toughening mechanisms are undoubtedly complex and not fully established, and the uniqueness of the mechanisms are not demonstrated compared to the traditional alloys.

Therefore, the preparation mechanisms and phase formation criterion of HEAs are summarized in this article. Based on the influence factors of element content, temperature, magnetism, and pressure, the conditions and causes of phase transformation of HEAs were systematically analyzed, and the relationship between the influence factors and microstructure was explored. The mechanisms of strengthening and toughening were summarized, and the similarities and differences between the HEAs and the traditional alloy in the mechanism were analyzed, hoping to provide a theoretical basis for the optimization design of mechanical properties of the HEAs.

# 2 Preparation of HEAs

As a new material, HEA has been widely used in aerospace, biomimetic material, catalyst, and so on [31,32]. Li and Chen [31] reviewed the preparation methods of HEAs as catalytic materials. At present, the preparation methods of HEAs are diversified. For example, the bulk HEA is usually prepared by melting casting [4,33] or powder metallurgy [34,35]. Waseem *et al.* [34] prepared $Ti_x$WTaVCr HEA by ball milling and SPS. The HEA coating is prepared by laser cladding [36], thermal spraying [37], or cold spraying [38]. The HEA thin film is prepared by magnetic sputtering [39] or plasma sputtering [40]. Liao *et al.* [39] prepared nanocrystalline ($CoCrFeNiAl_{0.3}$) thin-film by magnetron sputtering.

To improve the properties of HEAs, the HEA matrix composites have attracted much attention. The difficulties in the preparation are the control of the interface, especially the HEA matrix composites reinforced by fiber reinforcements [41,42]. Mileiko *et al.* [41] pointed out that a good interface is the basis of fiber-reinforced HEA with high creep strength. In addition, HEA nanoparticle-graphene nanoplatelets (GNPs) composite exhibited high corrosion resistance performance [42].

## 2.1 Preparation method and forming mechanisms of HEAs

The melting and casting method is the most widely used liquid preparation method and the earliest method to prepare HEAs. The AlCrCoNiCu HEA first prepared by Yeh *et al.* [22] was produced by vacuum arc melting followed by copper mold casting. To ensure chemical uniformity, the melting is usually repeated about five times. However, the casting method is easy to lead to structural defects such as composition segregation and shrinkage cavity as well as coarse and uneven microstructure. In addition, HEAs have many components, the melting

points of each element are different, and the metals with large melting points cannot be prepared by arc melting, so the selection of materials is limited.

Rolling can destroy the casting structure of ingot. In the process of plastic deformation, coarse grains are uniformly broken. In addition, rolling can eliminate defects formed during casting, such as bubbles, cracks and porosity. Rolling welds materials under high temperature and high pressure to improve the density and mechanical properties. Therefore, rolling is widely used in the optimization of HEAs prepared by melting and casting [43,44]. Li [43] prepared carbon-doped CoCrFeMnNi HEA by melting and casting method and refined the grain by hot rolling, cold rolling, and annealing treatments, which significantly improved the mechanical properties of the HEA. Moreover, the strength of $(FeCoNiCr)_{94}Ti_2Al_4$ was significantly improved after rolling [45].

Mechanical alloying is a kind of powder preparation technology. There are two reaction mechanisms of mechanical alloying. On the one hand, alloying is realized by diffusion. The metal powder is deformed, fractured, and cold welded, and the high-density crystal defects and a large number of diffusion couples are produced in the powder. The powder is refined and exposed to the fresh surface, which reduces the diffusion distance and promotes the formation of alloying powder. At present, the preparation of HEA powder by mechanical alloying is mostly controlled by diffusion [46,47]. On the other hand, alloying is realized by explosive reaction, and the powder is continuously refined in the initial stage of ball milling, which accumulates energy and increases the contact area between powders. Once the critical condition of the reaction is reached, the metal powder reacts in a very short time and gives off a lot of heat to form the alloy powder. This method is often used to prepare reinforcements of HEAs [48,49].

Powder metallurgy is the most widely used solid state preparation method for HEAs. In 2008, the AlFeTiCrZnCu HEA with BCC structure was prepared by powder metallurgy for the first time [50], and then this preparation method began to be widely used in HEAs. HEAs prepared by powder metallurgy have a stable microstructure and avoid component segregation. It can be used to prepare materials with very different melting points. The preparation process mainly includes pulverizing, mixing, pressing, and sintering. The sintering methods commonly adopted for HEAs include conventional sintering [50], hot pressing sintering [51,52], isostatic pressing sintering [8], and spark plasma sintering [35,53].

The basic process of sintering can be divided into three stages. At the initial stage of sintering neck formation, through nucleation, growth, and other atomic migration processes, the contact points between the particles are converted into grain bonding, forming sintering neck. During the growth stage of the sintering neck, the atoms migrate to the sintering neck in large numbers, which lead to the enlargement of the sintering neck and the reduction in particle spacing. Grain boundary diffusion plays a leading role in this process. The final sintering stage is a slow process. As the grains grow up, the voids on the grain boundaries go through the process of shedding, spheroidizing, and shrinking, and the voids disappear. After sintering, the alloy realizes metallurgical bonding. Compared with mechanical bonding, the bonding strength is higher and the mechanical properties are better. Fu *et al.* [54] prepared the $Co_{25}Ni_{25}Fe_{25}Al_{7.5}Cu_{17.5}$ nano-HEA by casting method and SPS and found that the grain size prepared by powder metallurgy was much smaller than that prepared by casting method, and the yield strength was larger.

Spraying means that the coating material is dispersed into uniform and fine droplets under the pressure or centrifugal force and then moved to the substrate to form the coating. HEA is an ideal coating material because of its high strength, hardness, good wear resistance, and high temperature oxidation resistance [55,56]. In the FeCoNiCrCu HEA coating with Si, Mn, and Mo additions, the microhardness increases to 450 $HV_{0.5}$ [55]. The interface between the coating and the substrate affects the properties.

The mechanical bonding interface is formed by the mechanical connection of materials inlaid with each other, and the bonding force is weak. The reactive bonding interface is bonded by chemical bonds. The bonding strength is high, but the toughness is poor, and it is easy to peel off under impact load. The diffusion bonding interface is formed by heating and pressing to promote the diffusion of the interface, and there is a composition gradient between the interfaces. Metallurgical bonding interface is metal bonding, which has high bonding strength, can bear the large external load, and is not easy to peel off. Liu *et al.* [57] prepared the $Al_2CoCrCuFeN$ HEA layer with 150 μm thickness on the H13 steel substrate. The interface was metallurgical bonding. The HEA coating significantly improved the surface hardness and high temperature wear resistance.

Magnetron sputtering is the most common method to prepare HEA films. The high-energy particles impact the target material and go through a complex scattering process in the target, collide with the target atom, and transfer momentum. The target atom gains enough momentum to move outwards and is sputtered out from the target surface. The target atoms collide with the

substrate, undergo the process of adsorption and desorption, surface migration, nucleation, and growth on the surface of the substrate to form a thin film. Under the action of the orthogonal electromagnetic field, the secondary electrons spin precession on the surface of the target material and fall onto the substrate after the energy is almost exhausted. Therefore, the damage of the film is reduced.

HEA films usually have high hardness [39,58]. Liao *et al.* [39] pointed out that the high hardness of the CoCrFeNiAl$_{0.3}$ nano-HEA thin films prepared by magnetron sputtering is due to the formation of nanostructure and the characteristic of selective growth. Several preparation methods of HEAs are shown in Figure 1. In this article, the corresponding preparation methods of different HEAs are summarized as shown in Table 1.

## 2.2 Interface improvement methods for HEAs and reinforcements

The HEA matrix composites are usually prepared into bulk materials by casting or powder metallurgy, but the difficulty lies in the regulation of the reinforcement, and the dispersion of the reinforcement and the regulation of the interface between the reinforcement and the matrix plays a key role in the performance of the HEA matrix

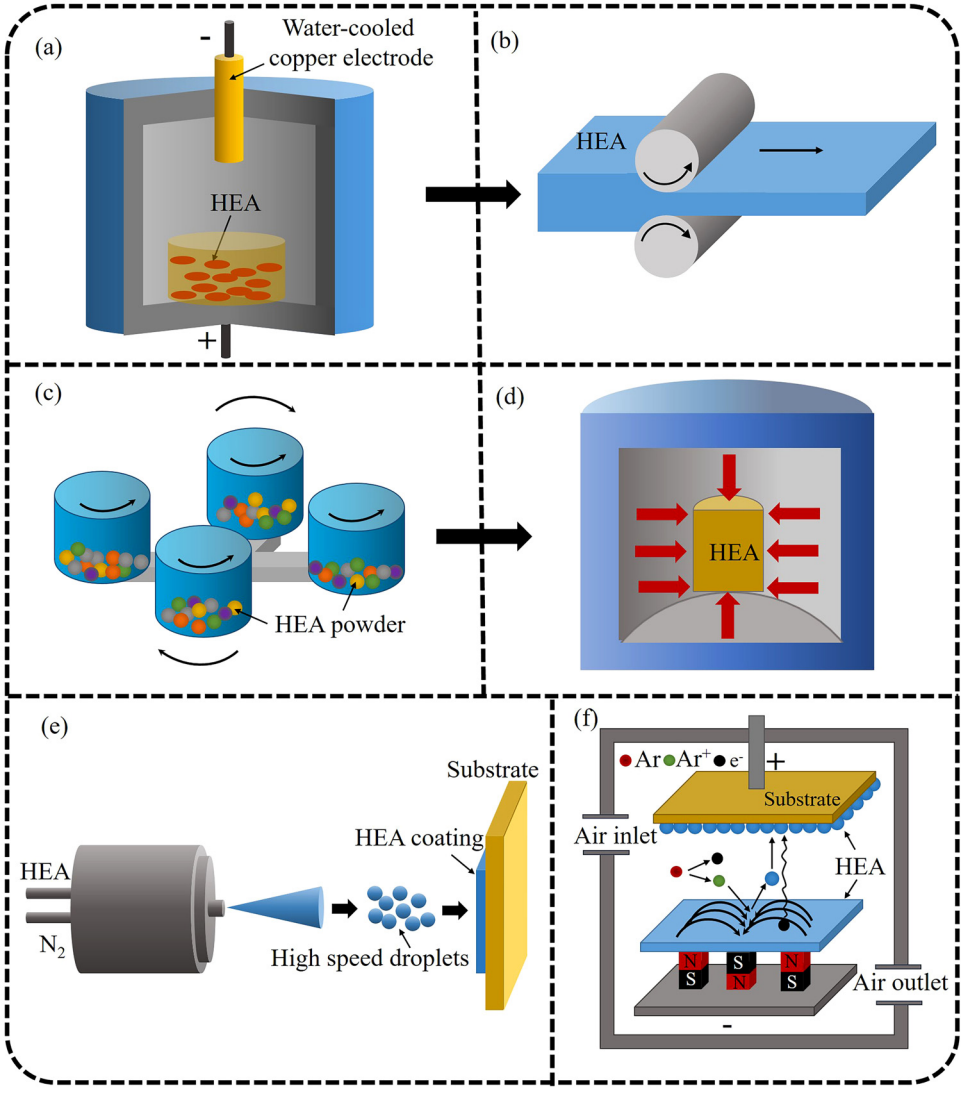


**Figure 1:** Schematic diagram of the preparation method of HEAs: (a) arc melting, (b) rolling, (c) mechanical alloying, (d) sintering, (e) spraying, and (f) magnetron sputtering.

**Table 1:** Summary of preparation methods of different HEAs

| Preparation method | HEAs | Reference |
|---|---|---|
| Melting-casting + rolling | CoCrFeMnNi | [43] |
| | $Fe_{40}Mn_{40}Co_{10}Cr_{10}$ | [44] |
| | FeCrNiCoMn | [59] |
| | FeCoNiCr | [45] |
| | $(FeCoNiCr)_{94}Ti_2Al_4$ | [45] |
| | FeMnCoCrCu | [60] |
| Mechanical alloying + powder metallurgy | NbMoCrTiAl | [47] |
| | CoCrFeNi | [61] |
| | CrMoNbWTi | [6] |
| | AlCoCrCuFeNi | [62] |
| | AlCuSiZnFe | [53] |
| | NbTaTiV | [34] |
| | NbMoTaWVCr | [63] |
| Spraying | AlCoCrFeNiTi | [37] |
| | CoCrFeNiAl | [56] |
| | CoCrFeNiMo | [56] |
| Magnetron sputtering | $CoCrFeNiAl_{0.3}$ | [39] |
| | CrNbTiMoZr | [64] |
| | CoCrFeNi | [65] |

composites. Because the dispersion of the reinforcements affects the wettability and interfacial bonding strength, thus affecting the mechanical properties. At present, the methods to improve the dispersion of the reinforcements of HEAs are mainly as follows:

(1) Mechanical stirring methods [29,66]. High energy ball milling is one of the most commonly used methods. Yang *et al.* [27,29] mixed nano-$Al_2O_3$ particles with the HEA powder by high-energy ball milling and then SPS sintering. Nano-$Al_2O_3$ particles were uniformly distributed in the matrix. Moreover, due to the uniform distribution of reinforcements and close combination with the matrix, the composite material had excellent mechanical properties. Liu *et al.* [67] added GNPs to the HEA powder for ball-milling for 8 h to obtain the uniformly distributed reinforcement, and found that when the content of GNPs reached 0.8 wt%, the agglomeration phenomenon was more obvious, and the strength and toughness of the composite material decreased.
(2) Surface modification [68,69]. Nano-fiber reinforcement is easy to agglomerate, such as carbon nanotubes (CNTs) and GNPs, because of van der Waals force. The surface modification was achieved by grafting functional groups on the surface of the fiber to enhance dispersibility. Rekha *et al.* [42] placed a mixture of the HEA powder and GNPs in a mixed solution of alcohol and sodium dodecyl sulfate and then achieved uniform distribution of GNPs by ultrasonic stirring. Some scholars also adopted the method of ultrasonic treatment of CNTs by placing them in an acid mixture ($H_2SO_4$:$HNO_3$ = 3:1) [68,69].
(3) *In situ* method [70,71]. Yang *et al.* [49] prepared $Al_{0.3}FeNiCo_{1.2}CrCu$ HEA with TiC by the *in situ* method. Ti, C and Al were dry mixed for 10 h to form TiC, and then mixed with other metal powders for 45 h, which can prevent the reaction of C with Fe or Co. A clean interface is formed between TiC and the HEA. *In situ* TiC-reinforced $(FeCrNiCo)Al_xCu_Y$ HEA was also prepared by Fan *et al.* [48]. The TiC is uniformly distributed and has good wettability with the matrix. Sun *et al.* prepared the FeCoNiCu HEA [70] and $Al_x$FeCoNiCu HEA [71] reinforced by *in situ* TiC, and the strength of the HEAs was obviously improved.

# 3 Phase formation and phase transformation mechanisms of HEAs

The phase of the material is closely related to the properties. At present, HEAs mainly have the solid solution type and the amorphous type. The criteria for phase formation of HEAs have been preliminarily studied. In addition, some HEAs undergo phase transformation under some conditions, and the mechanisms of phase transformation has not yet formed the system. At present, the main factors affecting the microstructure of HEAs are elements, temperature, magnetism, and pressure. It is significant to summarize how these factors affect the microstructure of HEAs and to analyze why they have such effects.

## 3.1 Criteria for phase formation

Hume-Rothery rule points out that the formation of binary solid solution is related to the atomic size difference, electronegativity, and valence electron concentration (VEC) [72,73]. The difference between electronegativity and atomic size of elements is small, which is beneficial to increase the solid solubility. A small absolute enthalpy of mixing means that the chemical properties of the elements are similar. The higher the mixing entropy, the lower the Gibbs free energy and the more favorable to form a solid solution. At present, some progress has been made in the criterion of the solid solution phase formation of HEAs.

Yang and Zhang [74] predicted whether HEAs could form solid solutions by two parameters: Atomic size difference ($\sigma$) and the special ratio of mixing entropy and mixing enthalpy ($\Omega$). The two parameters can be calculated by the equations (1–6). When $\Omega \geq 1.1$ and $\sigma \leq 6.6\%$, HEAs could form solid solution. Guo and Liu [9] also pointed out that the solid solution of HEAs is related to $\sigma$, $\Delta H_{\text{mix}}$, and $\Delta S_{\text{mix}}$. When $0 \leq \sigma \leq 8.5\%$, $-22 \leq \Delta H_{\text{mix}} \leq 7\ \text{kJ mol}^{-1}$, and $11 \leq \Delta S_{\text{mix}} \leq 19.5\ \text{J (K mol)}^{-1}$, HEAs could form a solid solution.

$$\sigma = \sqrt{\sum_{i=1}^{n} C_i(1 - r_i/r)^2}, \tag{1}$$

$$r = \sum_{i=1}^{n} C_i r_i, \tag{2}$$

where $\sigma$ is the difference in atomic size, $C_i$ represents the atomic percentage, $r_i$ is the radius of the component, and $r$ represents the average atomic size of all components.

$$\Delta S_{\text{mix}} = -R\sum_{i=1}^{n} C_i \ln C_i, \tag{3}$$

$$\Delta H_{\text{mix}} = \sum_{i=1, i\neq j}^{n} 4H_{ij}^{\text{mix}} C_i C_j, \tag{4}$$

$$\Omega = T_{\text{m}}\Delta S_{\text{mix}}/|\Delta H_{\text{mix}}|, \tag{5}$$

$$T_{\text{m}} = \sum_{i=1}^{n} C_i (T_{\text{m}})_i, \tag{6}$$

where $H_{ij}^{\text{mix}}$ is the mixing enthalpy of the ideal solid solution of the binary alloy system, $\Omega$ indicates the specific ratio of mixing entropy and mixing enthalpy, $T_{\text{m}}$ represents the theoretical melting point of the alloy system, and $(T_{\text{m}})_i$ represents the melting point of the component.

The structure of the solid solution can be predicted by the VEC which is calculated by equation (7). When VEC $\geq$ 8, the HEA has FCC structure; When 6.87 < VEC < 8, the HEA has FCC and BCC mixed structure; When VEC $\leq$ 6.87, the HEA has BCC structure [10]. Fu *et al.* [54] calculated the parameters of $Co_{25}Ni_{25}Fe_{25}Al_{7.5}Cu_{17.5}$ HEA, which are $\sigma$ = 3.53%, $\Omega$ = 30.7, and VEC = 8.9. Therefore, it is predicted that the HEA can form FCC solid solution, which is consistent with XRD results. Ni–Co and Fe–Ni have high solid solubility for other elements and can form FCC solid solutions. Cu and Ni have an infinite solid solution. Al has a high solubility in Cu. This is the fundamental reason for the HEA to form FCC solid solution. Chen *et al.* [75] used the same method to calculate the parameters of NbMoCrTiAl HEA, which are $\sigma$ = 5.4%, $\Omega$ = 2.92, and VEC = 4.8. Therefore, the BCC structure is predicted, which is consistent with the XRD, proving that the phase formation criterion is applicable. Figure 2 shows the influence of VEC on the structure of HEAs [76], which is consistent with VEC criterion.

$$\text{VEC} = \sum_{i=1}^{n} C_i (\text{VEC})_i, \tag{7}$$

where VEC represents the VEC of the HEA and $(\text{VEC})_i$ represents the VEC of the component.

The Inoue rule indicates the conditions for the formation of an amorphous phase [77]: (1) The alloy contains at least three elements, which lead to slow diffusion of elements and lattice collapse due to excessive lattice distortion. Therefore, the high entropy effect promotes the formation of the amorphous phase. (2) The ratio of the atomic radius of each component must be more than 12%. The difference of atomic radius is large, the internal

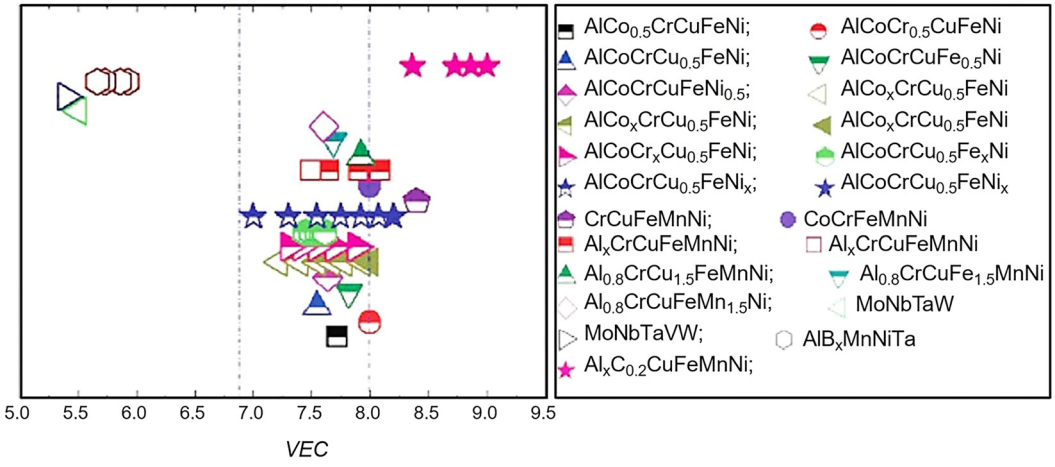


**Figure 2:** Relationship between VEC and solid solution stability of HEAs [76].

stress of lattice is large, and the solid solution is unstable. (3) The mixing enthalpy of any two main elements is very negative, which can promote the formation of short-range ordered structure of multielement clusters [78], which is conducive to the amorphous forming ability of the alloy.

When $\sigma \geq 9\%$, $-35 \leq \Delta H_{mix} \leq -8.5\ kJ\ mol^{-1}$, and $7 \leq \Delta S_{mix} \leq 14\ J\ (K\ mol)^{-1}$, the amorphous phase is formed in the HEA [9]. Many HEAs containing Zr are amorphous, most of which are less than 3 mm in diameter [79,80]. High entropy amorphous alloys usually have some special properties; for example, $Zn_{20}Ca_{20}Sr_{20}Yb_{20}(Li_{0.55}Mg_{0.45})_{20}$ exhibits homogeneous flow at room temperature and 25% plasticity [81]. Figure 3 shows the factors influencing the phase formation of HEAs [9,74,77,82]. HEAs mainly include the solid solution region and the amorphous phase region. Intermetallic compounds tend to form with the solid solution or amorphous alloys, especially between these two regions.

## 3.2 Effect of elements on phase formation

At present, the preparation of HEAs by powder metallurgy has been widely used. Some progress has been made in the study of the alloying sequence of elements during ball milling. The alloying rate is inversely proportional to the melting point, because the element with a low melting point in the solid state has a larger diffusion coefficient and a faster diffusion rate, which is more conducive to alloying. When the melting point is close, the alloying rate is proportional to the brittleness of the pure element, because the brittleness of the metal is more likely to be broken during ball milling, speeding up the alloying process. Furthermore, the lower the concentration of components, the faster the alloying rate [83]. The XRD analysis of the HEA powders with different milling times shows that the alloying sequence of the common elements in HEAs is Al → Cu → Co → Ni → Fe → Ti → Cr → Mo [54,83].

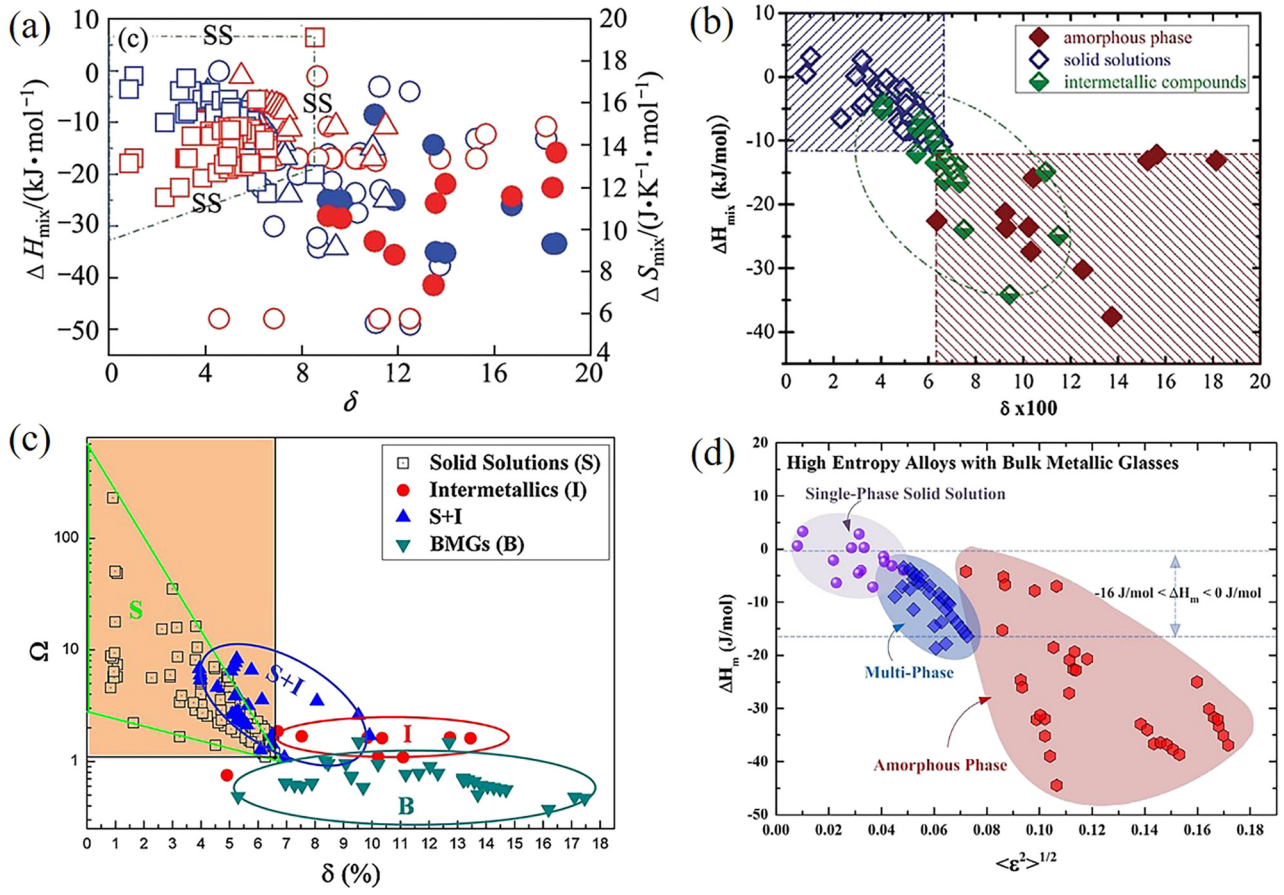


**Figure 3:** Relationship between the structure of HEAs and parameters, (a) superimposed effect of $\Delta H_{mix}$, δ and $\Delta S_{mix}$ [9], (b) superimposed effect of $\Delta H_{mix}$ and δ [77], (c) superimposed effect of Ω and δ [74], (d) superimposed effect of $\Delta H_m$ and $<\varepsilon^2>^{1/2}$ ($<\varepsilon^2>^{1/2}$ is the residual strain, which is related to δ) [82].

The phase structure of HEAs after alloying is related to the type and content of elements, such as Ti, Al, and V that can promote the formation of BCC structure, while Cu and Co can promote the formation of FCC structure [84]. Yang *et al.* prepared $Al_{0.4}FeCrCoNi_{1.2}Ti_{0.3}$ [27] and $Al_{0.4}FeCrCo_{1.5}NiTi_{0.3}$ [29] reinforced by nano-$Al_2O_3$ particles. The former was FCC + BCC structure, and the latter mainly was the FCC structure. The difference in microstructure is mainly related to the content of Co, and the less the Co content, the formation of the FCC structure is reduced. Al and Ti cannot be completely dissolved in FCC structure, and incompletely dissolved Al and Ti form bcc structure. Varalakshmi *et al.* [85] found that CuNi, CuNiCo, and CuNiCoZn were all FCC structures, and CuNiCoZnAlTi nano-HEA was BCC, which proved that Al and Ti promoted the formation of BCC structures.

The type and content of elements affect the alloying behavior and lead to phase transformation. The $CuCoNiCrAl_xFe$ was prepared by Yeh *et al.* [22], with the Al content from 0 to 2.8 at%, and the HEA changed from FCC to BCC structure. The effect of Al content on the hardness and lattice constant was also proposed, as shown in Figure 4(a). In addition, in the $Ti_{0.5}CrFeCoNiAl_xCu_{1-x}$ HEA [23] and $(FeCoNiCrMn)_{100-x}Al_x$ HEA [86], the microstructure changed from FCC to BCC with the increase in the Al content, as shown in Figure 4(b). The large radius of Al atom increases the lattice distortion energy and makes FCC unstable. The stacking density of BCC (68%) is lower than that of FCC and HCP (74%), which makes it easier to adapt to larger atoms. Alaneme *et al.* [76] pointed out that the phase structure of $Al_{0.5}CoCrCuFeNiV_x$ changed from FCC to BCC with the increase in V, which indicates that V element can promote the stability of BCC structure. The phase structure of CoCrFeNiNbx changed from FCC to FCC + HCP with the increase in Nb.

## 3.3 Effect of temperature on phase formation

The temperature of heat treatment or sintering also affects the phase transition of HEAs. The solid solution formed after alloying is in a metastable state, and the internal stress is released in the process of high temperature sintering or heat treatment, and the metastable structure is transformed into a stable one. At present, the preparation of HEAs mostly adopts SPS, because the rapid sintering process is in a non-equilibrium state, and a large pulse current may lead to the generation of uncertain phase structure [87]. In the process of heat treatment or sintering, $\eta$ and $\sigma$ may be produced, which are related to VEC.

FCC + BCC metastable solid solution of CoCrFeNiMn was formed after ball milling for 60 h, but the phase structure after SPS was only FCC, and the alloy powder transformed into a more stable phase during high temperature sintering [88]. The phase transformation of $Fe_{40}Mn_{40}Co_{10}Cr_{10}$ from FCC to HCP happened at 77 K, and proved that HCP phase is more stable at low temperature [89]. The HCP of CoCrFeMnNi was reversed to FCC when heated at different pressures, indicating that the FCC is stable at higher temperatures [90]. The $Al_{0.6}CrFeCoNi$ HEA underwent a phase transition from FCC to BCC at heat treatment temperatures of 800 and 1,000°C [91]. Ji *et al.* [87] suggested that CoCrFeNiAl was BCC after ball milling for 30 h. After annealing at 900°C, alloy powder was FCC structure. After SPS, the phase changed

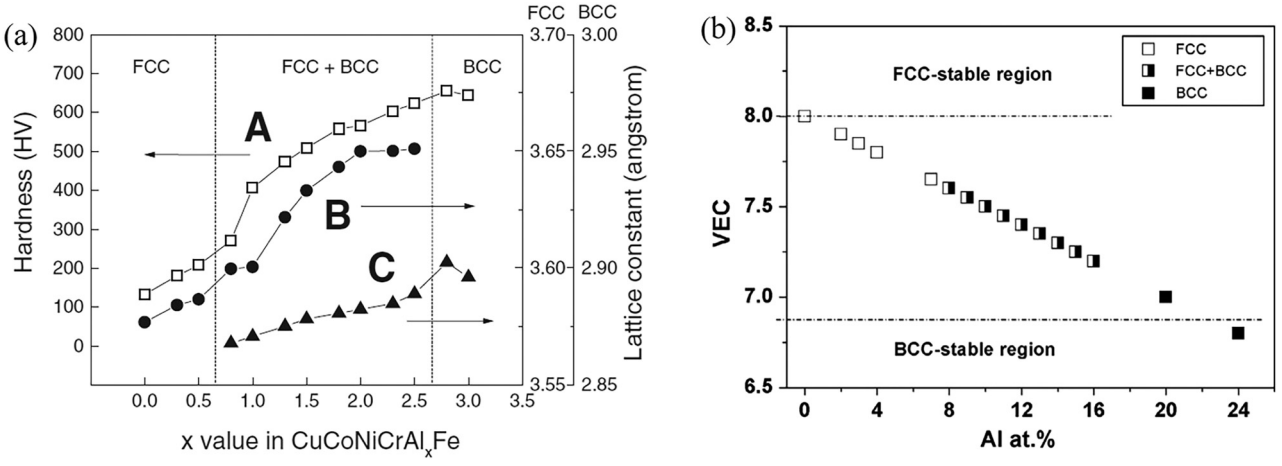


**Figure 4:** Effect of Al content on the structure of BCC and FCC in HEAs, (a) $CuCoNiCrAl_xFe$ HEA [22], (b) $(FeCoNiCrMn)_{100-x}Al_x$ HEA [86].

from BCC to FCC + BCC. Therefore, phase transformation happened during high temperature annealing and SPS.

## 3.4 Effect of magnetism on phase transition

At present, magnetically regulated phase transitions mainly refer to the transition between FCC and HCP. FCC stacking is ABCABC stacking, while HCP stacking is ABABAB stacking. The only difference between these two stacking methods is in stacking order. Therefore, the transition between the two only requires a small atomic displacement to form stacking faults, and the phase transition can be achieved locally. In addition, the stacking fault energy of HEAs is usually low, so the energy difference between FCC phase and HCP phase is small [24,25]. The Ab initio calculation shows that the FCC phase of CoCrFeMnNi HEA is stable relative to the HCP structure under magnetic condition. However, in the absence of magnetism, the HCP structure is predicted to be in the lowest energy state, that is, HCP is the most stable [92].

Li *et al.* [13] suggested that the decrease in Mn content is beneficial to the existence of HCP phase in HEAs. Niu *et al.* [25] compared the microstructure of CrCoNi and CrMnFeCoNi alloy, and CrCoNi alloy obviously had HCP structure. The effect of magnetism on HCP and FCC energies of the two alloys was observed. The HCP energy was always lower than FCC energy in CrCoNi, and the energy difference between the two phases had little change with magnetism, as shown in Figure 5(a). However, the energy difference between the two phases of CrMnFeCoNi decreased with the increase in the magnetic field, and the overlapping region appeared, as shown in Figure 5(b). This is related to the change in the magnetic moment of Mn between positive and negative. Pure Mn is an antiferromagnetic element. However, when Mn is combined with ferromagnetic elements Ni, Co, Fe and another antiferromagnetic element Cr, its preferred orientation of reverse arrangement cannot be completely satisfied. Therefore, the energy difference cannot be completely eliminated.

The effect of magnetism on the HCP and FCC energies of ternary derivatives of CrMnFeCoNi was further observed, as shown in Figure 5(c and d). It is proved that the energy difference between HCP and FCC phases can be eliminated by adding Mn atoms under the effect of magnetism, and Mn atoms can be arranged in parallel or antiparallel, so there is no driving force for FCC to HCP phase transformation in these alloys. Therefore, the addition of Mn inhibits the phase transition of the alloy from FCC to HCP.

## 3.5 Pressure-induced phase transition

Pressure is the driving force for the formation of defects and strains, which leads to the sliding of the atomic layer.

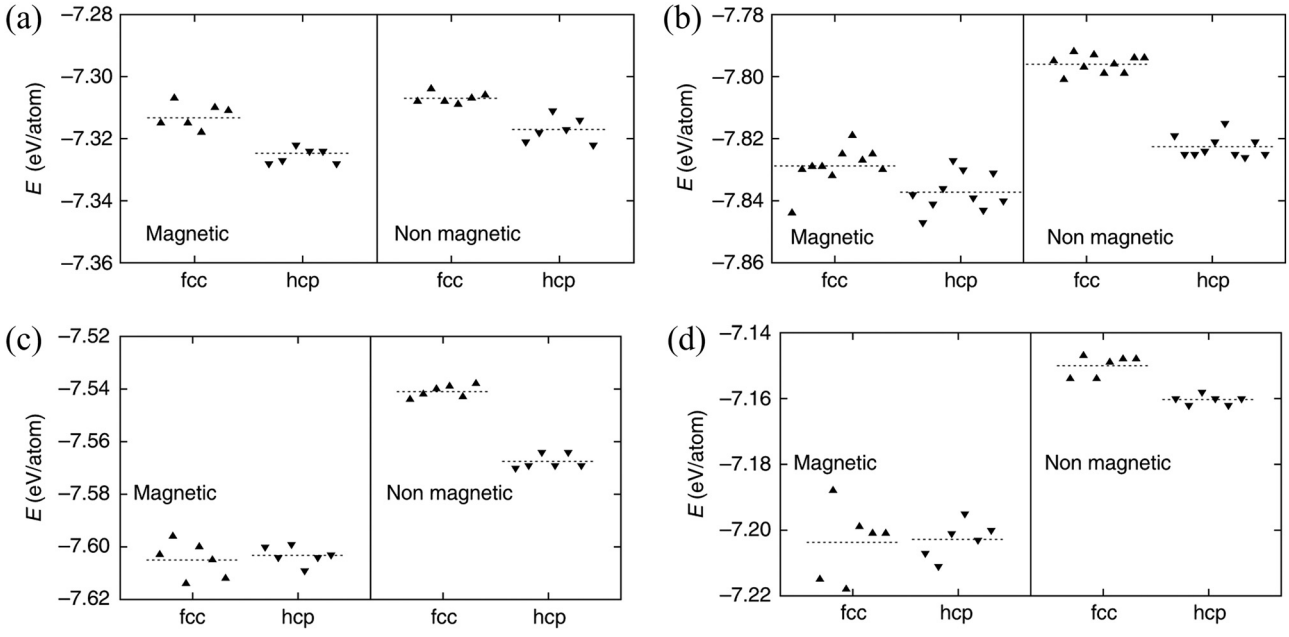


**Figure 5:** Effect of magnetic properties on the free energy of HCP and FCC phases in alloys: (a) CrCoNi, (b) CrMnFeCoNi, (c) NiFeMn, and (d) NiCoMn [25].

The stacking of FCC and HCP crystal structures is very close, the transition only needs atoms moving along {111} plane, and little thermal activation energy [93]. Therefore, pressure can drive the formation of defects and increase deformation and then promote the martensitic transformation. Li *et al.* [13] indicated that the transformation mechanism of $Fe_{80-x}Mn_xCo_{10}Cr_{10}$ is mainly deformation-induced martensite transformation. Zhang *et al.* [93] analyzed the phase transition of NiCoCrFe using *in situ* high pressure XRD. At 13.5 GPa, two new HCP diffraction peaks were found. The high pressure-induced FCC-HCP transition is slow, up to 39 GPa, and the FCC still has some left. Because the high pressure impedes atomic migration, thus kinetically inhibiting the martensitic transformation. Figure 6 shows the formation paths of HCP, Path 1 shows the formation and growth of twins, Path 2 shows the formation and growth of HCP phase from the intrinsic stacking fault, and Path 3 shows the formation and growth of HCP phase from the twin boundary [25].

Pressure can cause lattice distortion, change the stacking density of the lattice, even collapse the lattice, and promote the phase transition. Ahmad *et al.* [94] pointed out that the BCC structure of TiZrHfNb is still stable when the pressure reaches 50.8 GPa. Guo *et al.*

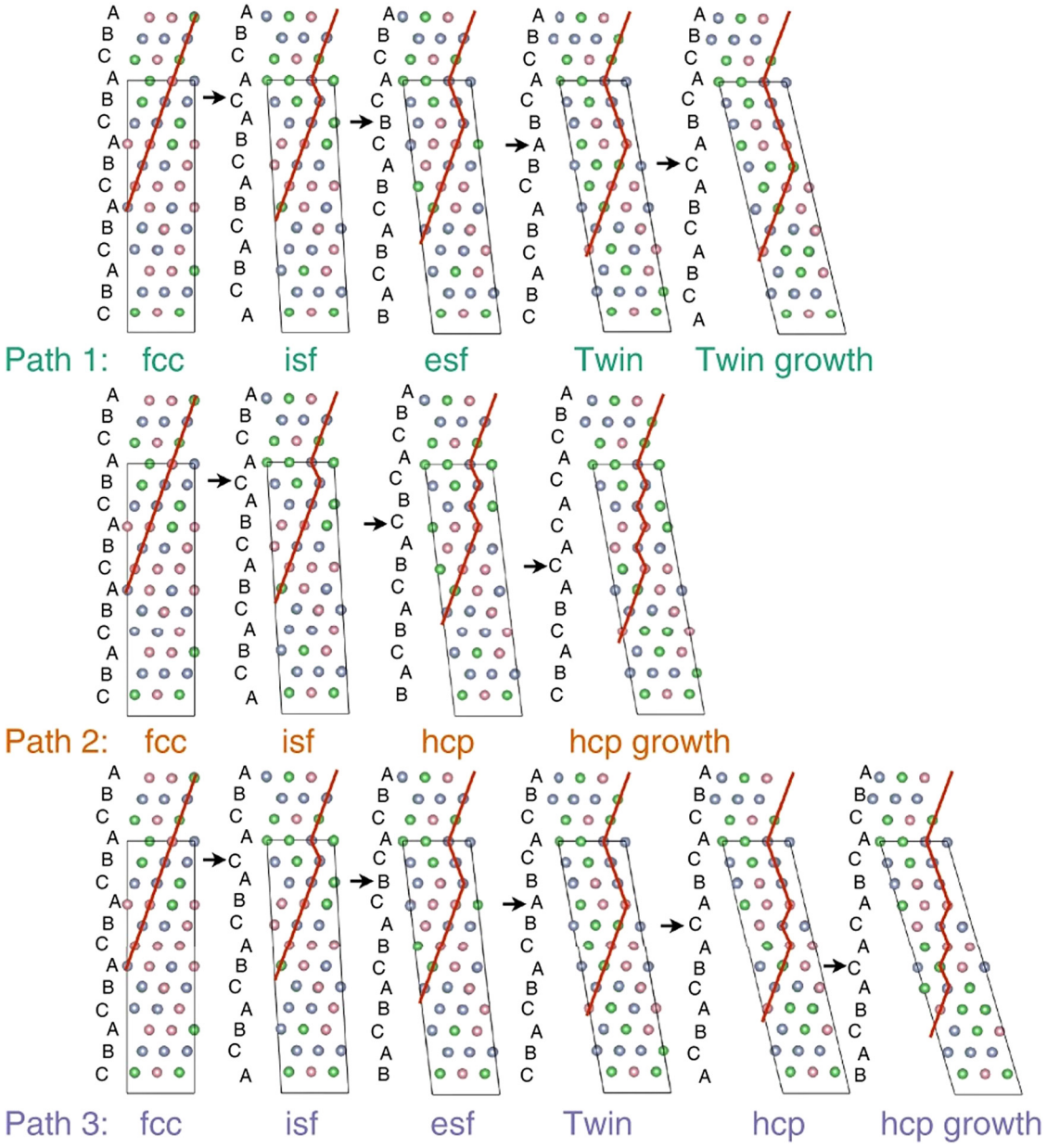


**Figure 6:** Schematic diagram of HCP phase formation paths [25].

[95] showed that when $(TaNb)_{0.67}(HfZrTi)_{0.33}$ was compressed to 100 GPa, the BCC structure did not undergo a phase transition. The results show that the BCC HEAs have good structural stability even at tens of GPa. According to the idea that content of Al can change the structure of $Al_xCoCrFeNi$ HEA, Cheng *et al.* [18] selected the components at the critical point of FCC and BCC phase transformation to reduce the phase stability of the HEA, and studied the phase transformation under high pressure. When the pressure reaches 17.6 GPa, a new peak appears on the (110) left shoulder, and its intensity increases at the expense of (110) peak, indicating that the high pressure-induced phase transition begins at about 17.6 GPa. The splitting of (110) peak is due to the severe lattice distortion caused by pressure, which leads to the phase transition.

The increase in pressure suppresses the magnetism of metal [96], and the high pressure causes the collapse of magnetic moment [24,97]. In addition, the pressure broadens 3D valence bands and reduces the density of Fermi energy level, which inhibits the magnetic moment [96]. The inverse proportional relationship between pressure and local magnetic moment in CrMnFeCoNi was confirmed by Ab initio calculations [92,98]. As mentioned above, the relative stability of FCC and HCP in CoCrFeMnNi HEA with or without magnetism is different. Therefore, high pressure inhibits the local magnetism and then promotes the transformation of HEAs from FCC to HCP. Tracy *et al.* [24] synthesized the HCP HEA by high pressure. Increasing pressure inhibited local magnetism, FCC instability, and the martensitic transformation began at 14 GPa, as shown in Figure 7(a). The HCP volume fraction increased with continued pressure, as shown in Figure 7(c). However, this phase transition was slow, because there was a proportional relationship between the pressure and stacking fault formation energy, and the high stacking fault energy slows down the transformation of the remaining FCC.

High pressure can induce the disordered and ordered transitions. There was a local short-range order structure (SRO) in HEAs [99,100]. Zhang *et al.* [100] used X-ray distribution function analysis and extended X-ray absorption fine structure (EXAFS) measurement to detect the local structure of NiCoCr, and found the short-range ordered structure. With the increase in pressure, the order degree of SRO increases. When the pressure reaches the critical value, SRO can be transformed into an ordered phase [99]. SRO and ordered phase are coherent, so the deformation energy of nucleation is low. To increase the possibility of phase transition, Pr was added to the CoCrCuFeNi HEA [99]. The *in situ* high-pressure XRD indicated that the peak intensity of O-FCC (ordered) suddenly increased at 16.0 GPa, while that of D-FCC (disordered) decreased as shown in Figure 7(b), so the D-FCC transited to O-FCC. Figure 7(d) clearly shows that the O-FCC fraction increased rapidly from about 8 GPa, indicating that the pressure reached the critical value and SRO developed into an ordered phase. However, it changed slowly after 18.0 GPa, because the movement and diffusion of atoms were limited with the increase in pressure.

# 4 Strengthening and toughening mechanisms of HEAs

With the development of HEAs, some deficiencies have been exposed in the properties. For example, although the refractory HEAs have high strength, hardness, and good wear resistance, they have poor plasticity and toughness [8,101], such as the ReMoTaW HEA with the maximum strength of 1,451 MPa and the failure strain of 5.69% [101]. The traditional strengthening and toughening methods can be used for HEAs, but the research on the mechanisms of strengthening and toughening have not yet formed a system.

## 4.1 Several common strengthening mechanisms

Solid solution strengthening is mainly due to the difference in atomic size, solute atoms cause lattice distortion, produce stress field, and increase the resistance of dislocation movement, to achieve the effect of strengthening. It can be divided into interstitial solution strengthening and displacement solution strengthening, as shown in Figure 8(a). Solid solution strengthening mainly comes from the elastic interaction (size effect) and modulus interaction between dislocations and solute atoms, and the solid solution strengthening of HEAs can be superimposed [102,103]. Yeh *et al.* [22] pointed out that the reason for the high hardness of HEAs is that there is no concept of the matrix, and all atoms are solute atoms, which leads to the higher saturation degree of solid solution. Li [43] added a small amount of C atoms to the CoCoCrFeMoNi, and the interstitial C atoms increased the stress field, so it played a role in solution strengthening. The value of solid solution strengthening can be calculated by equation (8) [62,104]:

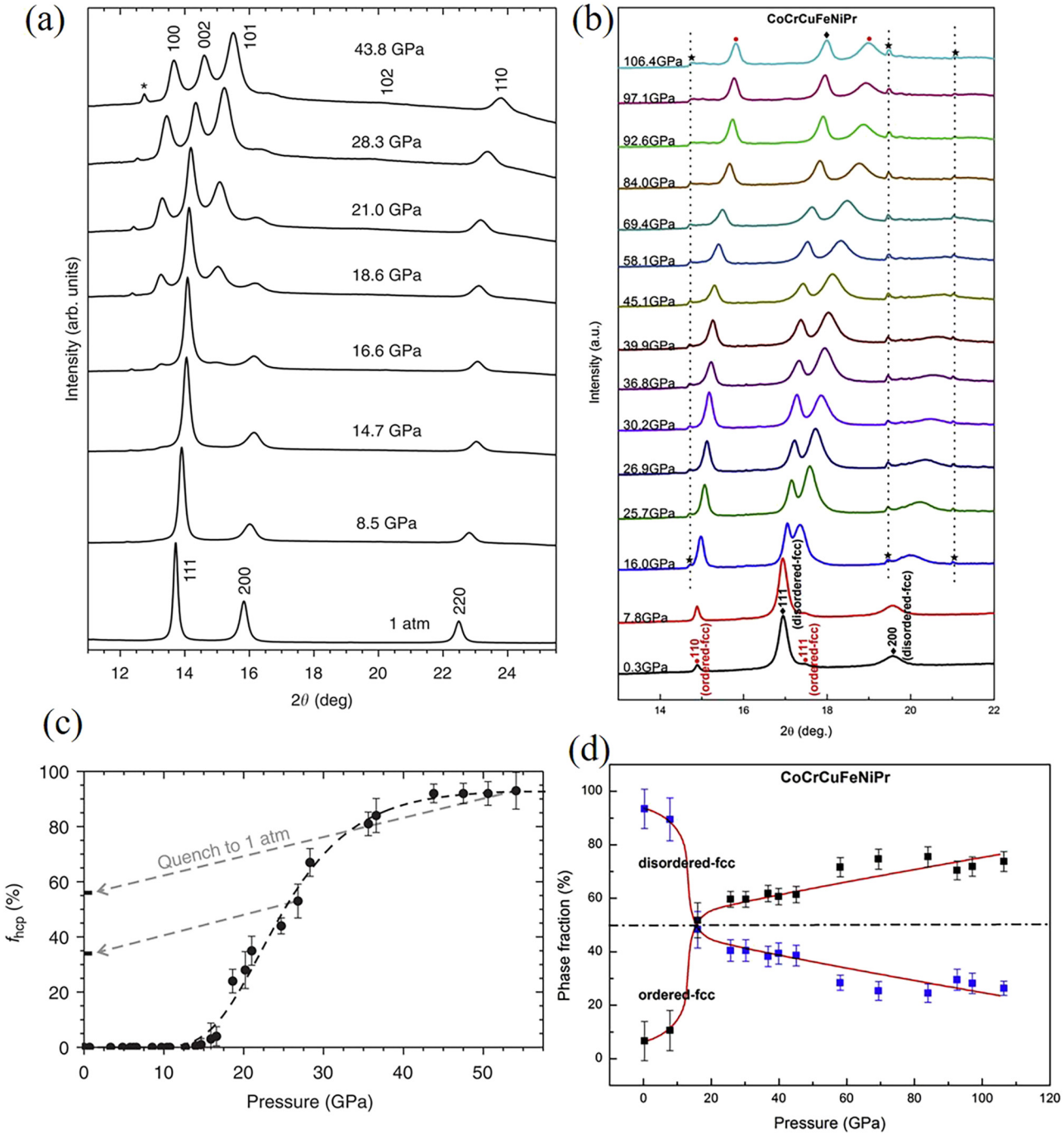


**Figure 7:** *In situ* high-pressure x-ray diffraction patterns and phase fractions with pressure, (a and c) CrMnFeCoNi [24] and (b and d) CoCrCuFeNiPr [99].

$$\Delta\sigma_{SS} = AG\varepsilon^{4/3}C^{2/3}, \tag{8}$$

where $\Delta\sigma_{SS}$ is the solution strengthening value, $A = 0.1$, $C$ is the concentration of atoms in solution, $G$ is the shear modulus of the alloy, and $\varepsilon$ is the lattice distortion caused by the solution.

Fine-grain strengthening means that the strength can be increased by refining the grain size. Because of the thermal stability and hysteresis diffusion effect of HEAs, the grain is not easy to grow in the sintering process, and even HEA nanomaterials can be obtained. For example, the grain size of $Co_{25}Ni_{25}Fe_{25}Al_{7.5}Cu_{17.5}$ after SPS is in the nanometer level [54]. In addition, the reinforcement of the HEA matrix composite has a hindrance to dislocation movement and interface migration, so the effect of fine-grain strengthening is obvious, as shown in Figure 8(b).

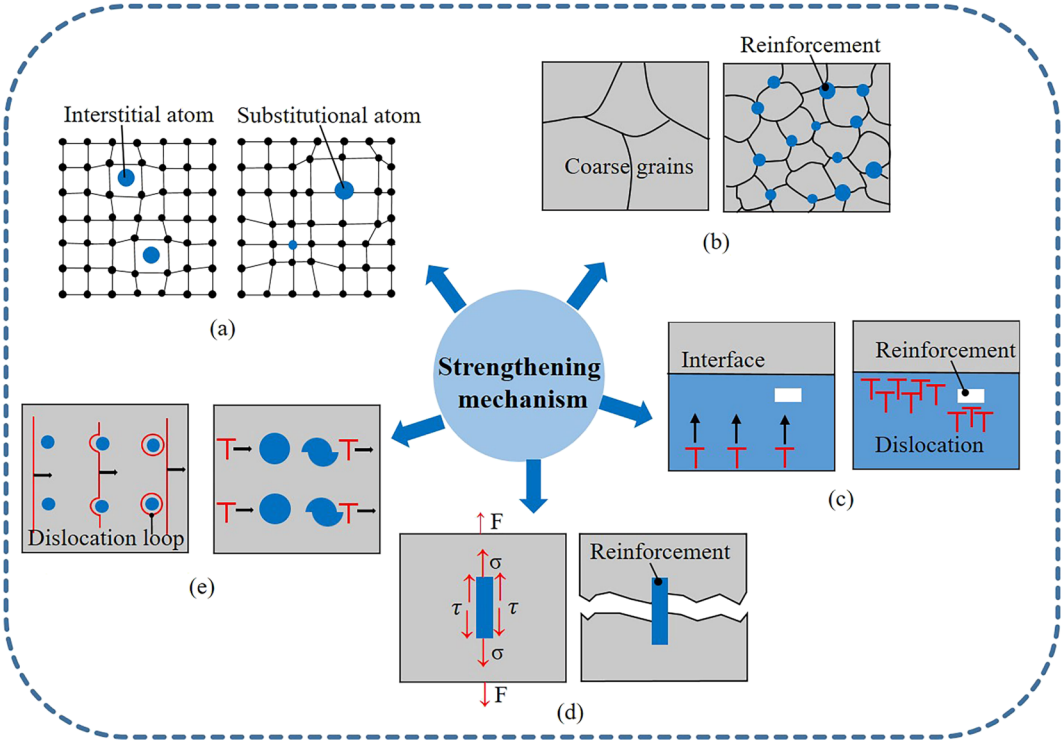


**Figure 8:** Schematic diagram of strengthening mechanism of HEAs, (a) solution strengthening, (b) fine grain strengthening, (c) dislocation strengthening, (d) load transferring, and (e) dispersion strengthening.

Wang *et al.* [105] showed that the addition of *C* in the HEA greatly hindered the grain growth, to achieve the effect of fine-grain strengthening. The fine-grain strengthening value of the HEA matrix composites can be calculated by equation (9) [54,62]:

$$\Delta\sigma_{GR} = K(d^{-0.5} - d_0^{-0.5}), \tag{9}$$

where $\Delta\sigma_{GR}$ is the fine-grain strengthening value, $K$ is the Hall–Petch constant, $d$ is the average grain size of the composite material, and $d_0$ is the average grain size of the HEA.

Dislocation strengthening refers to the mutual delivery and entanglement during dislocation movement, which forms the obstacle of dislocation movement and makes plastic deformation difficult, thus improving the strength, as shown in Figure 8(c). Deng *et al.* [44] prepared $Fe_{40}Mn_{40}Co_{10}Cr_{10}$ by melting, casting, hot rolling, and homogenization treatments. It was observed that there were a large number of active dislocations in the HEA. These dislocations overlapped and crisscrossed with each other, resulting in a high-density dislocation wall, which hindered the movement of dislocation. For the HEA matrix composites, due to the different thermal expansion coefficients of the reinforcement and the matrix, high-density dislocations are produced during processing, and the reinforcement hinders dislocation slip and grain boundary movement, to improve the strength. The dislocation strengthening value is calculated according to equation (10) [54,62]:

$$\Delta\sigma_{Dis} = M\alpha Gb\rho^{1/2}, \tag{10}$$

where $\Delta\sigma_{Dis}$ represents the dislocation strengthening value, $M$ and $\alpha$ of the FCC structure are 3.06 and 0.2, respectively, $G$ represents the shear modulus, $b$ represents the Berg vector, and $\rho$ represents the density.

The strengthening effect of load transfer is related to the interface between the reinforcement and the HEA matrix [106]. When subjected to stress, the matrix or interface is the first to fracture, and the reinforcement is pulled out and acts as the main load bearer. Because the strength of the reinforcement is much larger, additional force is needed to make the reinforcement break completely, so the strength increases [46,107], as shown in Figure 8(d). For fiber reinforcement, load transfer is a very important strengthening mechanism. At present, fiber reinforcement has been widely used in traditional metal matrix composites [106], but its application in the HEA matrix composites is very few. Liu *et al.* [67] prepared GNPs-reinforced HEA matrix composites by SPS sintering. It was pointed out that one of the reasons for

the high strength of the composites was that the load transferred from the HEA to the GNPs. The strengthening value of load transfer of HEA matrix composites can be calculated by equation (11) [67]:

$$\Delta\sigma_{LT} = f_v\sigma_m/2, \quad (11)$$

where $\Delta\sigma_{LT}$ is the load transfer strengthening value, $f_v$ is the volume fraction of the reinforcing phase, and $\sigma_m$ is the yield strength value of the matrix.

Dispersion strengthening means that the second phase particles hinder the movement of dislocations. According to the interaction between particles and dislocations, it can be divided into two types: one is Orowan strengthening mechanism where the particles are strong enough, the radius of the particles exceeds the critical value, and the dislocations bypass the particles. The other is the Ansel-Lenier mechanism, in which the dislocation cuts through the particles and the particles break. When the particles are small enough and coherent with the matrix, it is easy to occur [45,46,108], as shown in Figure 8(e). The $Fe_{25}Co_{25}Ni_{25}Al_{10}Ti_{15}$ precipitated $\gamma'$, the HEA and $\gamma'$ are coherent, and dislocation shear $\gamma'$ [46]. Fan *et al.* [48] prepared TiC-reinforced $(FeCrNiCo)Al_{0.7}Cu_{0.5}$, and the yield strength of the HEA was 630 MPa, and that of the composite was 1,290 MPa. The Orowan strengthening value of the HEA matrix composites can be calculated by equation (12) [67,109]:

$$\Delta\sigma_{Orowan} = \left\{0.13\, Gb/d_p\left[(2f_v)^{-\frac{1}{3}}-1\right]\right\}\ln(d_p/2b), \quad (12)$$

where $\Delta\sigma_{Orowan}$ is the Orowan strengthening value, $G$ is the shear modulus of the HEA matrix, $b$ is the Berger vector of the matrix, and $f_v$ and $d_p$ are the volume fraction and size of the reinforcement, respectively.

## 4.2 TRIP effect

Entropy-stable single-phase HEAs are often difficult to achieve and limit the development of strong and tough HEAs. In recent years, new dual-phase HEAs (DP-HEAs) have been designed to improve mechanical properties [13,110]. The strength of CrMnFeCoNi DP-HEA is much higher than that of single-phase HEA, and it maintains good toughness [110]. The TRIP-DP-HEAs indicate that the stability of the solid solution phase of HEAs is controllable, and the mechanical properties of non-equiatomic HEAs containing metastable phase can be improved by TRIP effect.

At present, most of the phase transition of TRIP-DP-HEAs is from FCC to HCP [111–113]. At the initial stage of deformation, 1/6 <112> Shockley partial dislocation slip forms stacking fault and a large number of stacking faults in the FCC matrix are superimposed as the core of HCP nucleation to realize the phase transition [114]. At the later stage of deformation, the increased interfacial density caused by the phase transition increases the barrier to dislocation slip, thus promoting strain hardening and ensuring that TRIP-DP-HEA is strong and tough. The microscopic process of phase transition of the TRIP-DP-HEA is shown in Figure 9.

The mechanical properties of TRIP-DP-HEAs are closely related to the metastability of FCC matrix, the initial fraction of HCP phase, the grain size of FCC matrix, and the stacking fault density [60,115]. The lower the stability of FCC matrix, the more conducive it is to ECAP effect. The higher the initial phase fraction of HCP, the higher the material strength and hardness, but increasing the initial phase of FCC is beneficial to TRIP effect. The decrease in grain size, the increase in grain boundary area per unit volume, and the number of preferred nucleation sites of HCP phase increase, which is conducive to TRIP effect. However, the decrease in grain size may lead to an increase in back stress, which seriously restricts the nucleation growth of HCP [116,117]. Stacking fault is the core of HCP nucleation, and the higher the stacking fault density, the more conducive HCP is to phase transition.

To reduce the stability of FCC phase in HEAs, it is usually adopted to change the composition concentration

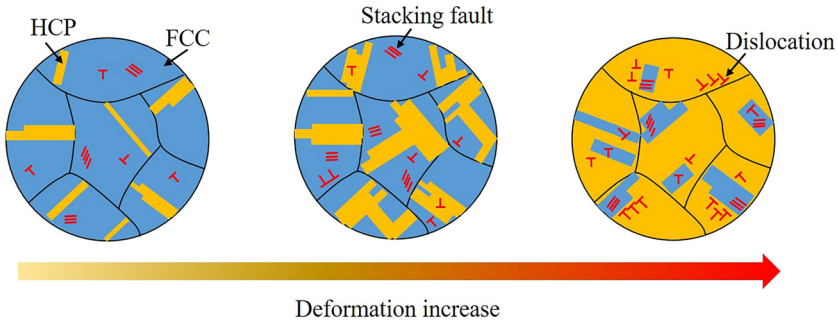


**Figure 9:** Schematic diagram of phase transition of the TRIP-DP-HEA.

to reduce the stacking fault energy [19,20]. Wei *et al.* [21] reduced the concentrations of Mn, Ni, and Fe in the HEA, increased the concentrations of Co and Cr, and reduced the SFE value according to ab initio and thermodynamics calculations. Based on the phase diagram and the Thermo-Calc simulations, Nene *et al.* [20] found that adding 5 at% of Si in $Fe_{42}Mn_{28}Co_{10}Cr_{15}$ can effectively reduce the phase stability of the FCC matrix and the SFE of the system, and promote the significant TRIP effect of the DP-5Si-HEA.

Friction stir processing (FSP) is a large plastic deformation technique, which can refine the grain size of the matrix and regulate and optimize the ratio of FCC and HCP phases of HEAs in the deformation process. Both the tensile strength and elongation of the $Fe_{50}Mn_{30}Co_{10}Cr_{10}$ DP-HEA treated with FSP increased, and EBSD and XRD results before and after deformation proved that deformation-induced the transformation of FCC to HCP [115]. Nene *et al.* [20] compared the changes in microstructure and properties of $Fe_{42}Mn_{28}Co_{10}Cr_{15}Si_5$ before and after FSP, and found that FSP significantly refined grain size, retained a different degree of strain, increased the store of dislocation, and promoted the transition from metastable FCC phase to HCP phase. However, the speed of FSP in this experiment decreased after each cycle, which restricted the further nucleation of HCP phase, stabilized the FCC phase in the tissue, and ensured the dominance of the initial FCC. The yield strength and plasticity of the HEA with FSP are improved compared with that of the as-cast HEA.

## 4.3 TWIP effect

The introduction of TWIP effect into HEAs can effectively improve the mechanical properties. Because Strain-induced twinning provides a supplementary deformation mechanism. The interconnection of the different twin systems in HEAs results in a mixed twin structure. By creating three-dimensional channels and some twin boundaries to allow dislocation cross slip, the stress caused by dislocation accumulation is reduced, and the plasticity and toughness of HEAs are further improved [19,118]. The interaction between twins and the barrier of twin boundary to dislocation increases the strength. The synergistic effect of these micro-deformation processes promotes the HEAs to have higher fracture resistance. The materials with twinning as the main deformation mechanism show high strength and plasticity [119,120]. TWIP effect is expected to be an important way of strengthening and toughening HEAs [121].

Zhang *et al.* [28] studied the effect of deformation twins on the plasticity of $AlCoCrFeNi_{2.1}$, and pointed out that the diffusion activation energy of a single atom at the twin boundary is half of that of its diffusion activation energy. The diffusion rate of atoms at the twin boundary is higher, and atoms at the twin boundary diffuse more easily and rapidly than atoms inside the grain. Therefore, the element diffusion in the deformation process makes the twin boundary more likely to migrate, thus increasing the ductility of the alloy. The TiC-reinforced $Al_{0.3}FeNiCo_{1.2}CrCu$ HEA were prepared by Yang *et al.* [49], and twins were found in the microstructure which was induced by high temperature and pressure in SPS, and TiC provides a fulcrum for the nucleation of deformation twins. The yield strength, fracture strength, plastic strain, and hardness of the HEA were improved.

The mechanism of twin formation in HEAs is not clear. It is generally believed that stacking fault can be the core of twin nucleation. The $Al_{0.3}CoCrFeNi$ HEA was observed with a large number of stacking faults around the stepped twin, which proves that stacking faults are the nucleation core of the twin [121], as shown in Figure 10. The mechanical properties of FeMoCoCr series HEAs can be improved by adjusting the deformation mechanism by changing element content, such as reducing Mo content or increasing Co content, which can reduce stacking fault energy. The plastic deformation mechanism changes from dislocation-dominated deformation to TWIP and then to TRIP, which proves that the directional stability can be achieved by adjusting the stacking fault energy [13,114]. Wei *et al.* [21] prepared the $Co_{35}Cr_{20}Mn_{15}Ni_{15}Fe_{15}$ and $Co_{35}Cr_{25}Mn_{15}Ni_{15}Fe_{10}$ HEAs by adjusting the composition concentration to reduce stacking fault energy, and the HEAs had significant TWIP effect and TRIP effect, respectively. The TWIP effect contributed more to plasticity, while TRIP effect contributed more to strength.

## 4.4 Crack bridging and crack deflection

Crack bridging refers to the bridging of reinforcements between crack planes after matrix cracking [118], which is equivalent to adding closure stress on crack planes, to prevent crack propagation and achieve the effect of increasing toughness, as shown in Figure 11(a). The reinforcement breaks until the applied stress reaches its fracture strength [122,123]. Crack deflection refers to that when the interface is weak or the obstacle is strong enough to prevent the crack from passing through, the

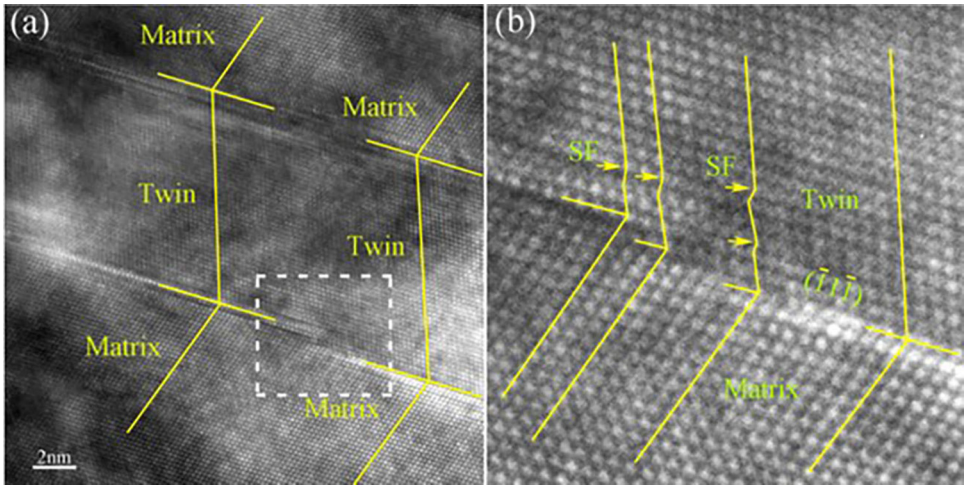


**Figure 10:** The HRTEM image of $Al_{0.3}CoCrFeNi$, (a) a typical deformation twin and (b) the enlarged image of the white dashed square in (a) [121].

crack deviates from the original direction and bypasses the obstacle, expanding along with the interface, or even bifurcate. Because the crack changes the expansion path and absorbs the energy of the fracture, the toughening effect is achieved [123,124], as shown in Figure 11(b). $TiB_2$-TiNiFeCrCoAl HEA showed good fracture toughness which is due to the crack bridging, crack deflection, and branching [123]. Luo *et al.* [124] observed crack bridging and deflection in WC-$Al_x$CoCrCuFeNi composites.

Li *et al.* [118] observed the crack bridging phenomenon in the last stage of crack propagation of the micron-sized CrMnFeCoNi with FCC phase structure. Nano-fibers were formed behind the crack tip, which connected the two crack surfaces behind the crack tip and effectively inhibited the crack opening. Therefore, the opening of cracks is accompanied by the deformation of many nano-fibers, which provide a stable source for the toughening of the HEA. Further propagation of the crack tears the nano-bridge and activates the nano-scale twins as the main deformation mechanism.

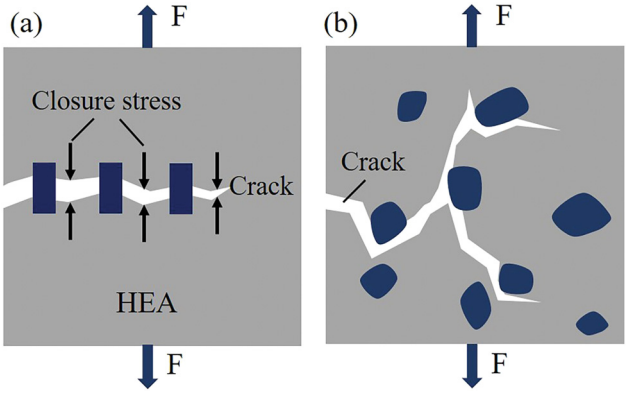


**Figure 11:** Schematic diagram of (a) crack bridging and (b) crack deflection mechanisms.

Kim and Kim [125] pointed out that for short and sharp cracks, the crack deflection at the twin boundary and the plastic relaxation caused by twins and decrystallization are the main ways to hinder the crack propagation. For the larger crack, the crack passivation and bridging action at the deformation twin block the crack propagation. *In situ* tensile TEM of the $Cr_{26}Mn_{20}Fe_{20}Co_{20}Ni_{14}$ DP-HEA showed that nano-twins play an important role in improving the toughness and inhibiting cracking. In Figure 12(a and b), the nano-twins nucleated and propagated in front of the crack tip, making the crack tip passivated, as shown in Figure 12(c and d). As the strain increased, the crack deflected along the twin shear direction, and the crack surface showed a zigzag shape, as shown in Figure 12(e and f) [126]. In addition, the FCC precipitates in the AlCoCrFeNi HEA strengthened the BCC grain boundary, resulting in the serious blocking of the crack at the BCC grain boundary, so the crack bifurcation phenomenon occurred and the crack propagation direction was changed [127].

## 4.5 Toughening of concentration wave and dislocation motion

Concentration wave refers to the obvious concentration fluctuation in HEAs, which plays a key role in high strength and good ductility. The distribution of elements

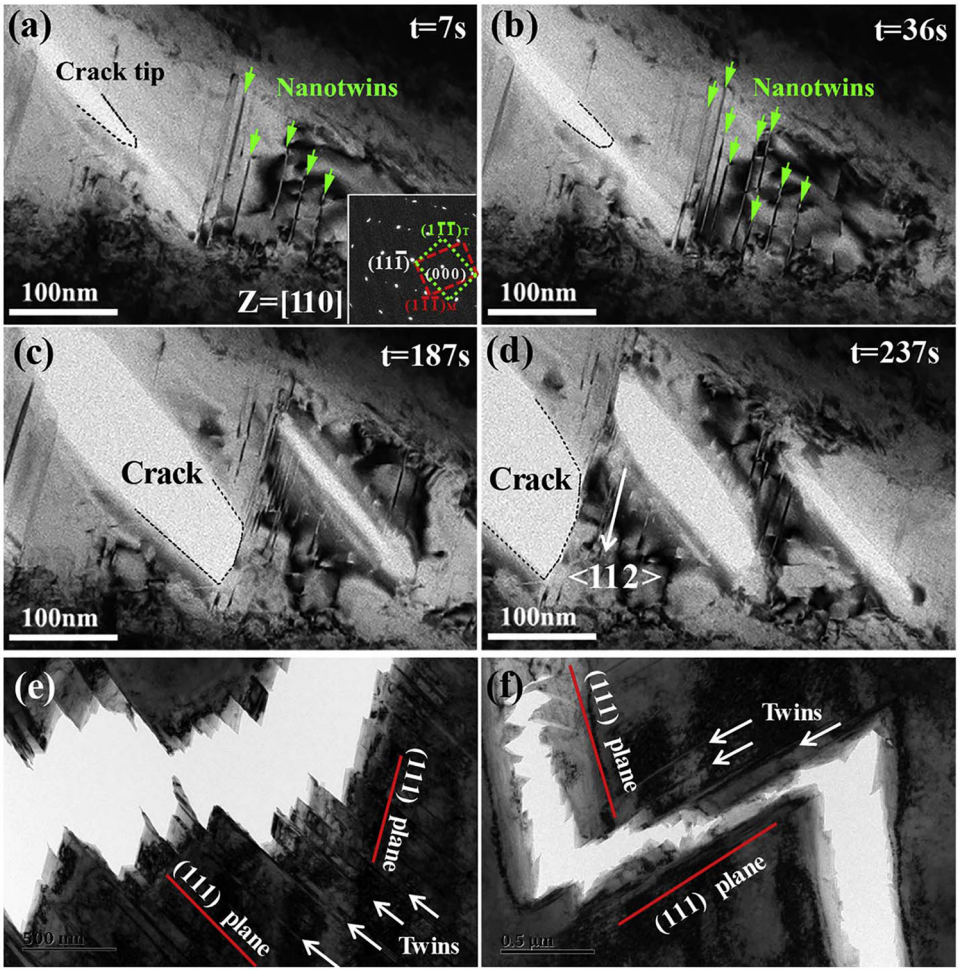


**Figure 12:** *In situ* TEM images of the area around a crack tip of the $Cr_{26}Mn_{20}Fe_{20}Co_{20}Ni_{14}$ during the tensile test, (a and b) at the initial steps, nano-twins were visible, (c and d) as the tensile process continues, bridging deflection and blunting occurred, (e and f) at the post-deformation, a crack appeared jagged [126].

in HEAs is not uniform on the lattice scale, and the concentration wave is ubiquitous, which makes HEAs different from the traditional alloys [128,129]. Ding *et al.* [129] found the mechanism of the concentration wave controlling the strength and toughness. To amplify the concentration fluctuation, the Mn in CrMnFeCoNi was replaced by Pd. The atomic size and electronegativity of Pd are different from other elements. Pd is more prone to form intermetallic compounds. Therefore, the addition of Pd promotes its separation from the other four elements, resulting in obvious chemical inhomogeneity in the HEA. Compared with the element line distribution of the two alloys, the atomic fraction of each element of CrFeCoNiPd fluctuated more greatly, and the atomic fraction of Pd fluctuated up to 58%. It is also because of the sharp concentration fluctuation of element distribution that the dislocation of the CrFeCoNiPd HEA can maintain a continuous and small movement, promote a large number of cross slips, and improve the mechanical properties.

In many FCC metals, the deformation carrier is mainly the dislocation movement, which is the cause of plastic deformation at the crack tip. Dislocation emission from the crack tip leads to the passivation of the crack tip, and the possibility of brittle fracture is reduced. Therefore, dislocation movement provides a strong toughening mechanism for HEA mainly through crack tip passivation [118]. This phenomenon is proved in the CrMnFeCoNi HEA [130].

Zhang *et al.* [130] carried out an *in situ* TEM strain test on the CrMnFeCoNi HEA with cracks. At the initial stage of deformation, it was observed that there are 1/6 <112> Shockley partial dislocations in the crack tip which move rapidly. With larger deformation, a large number of partial dislocations nucleate and proliferate on the {111} slip surface. Due to the low stacking fault energy of the HEA, a large number of stacking faults are formed. Stacking

faults react with each other. Three pairs of parallel stacking faults form a stacking fault parallelepiped, which strongly hinders dislocation movement and promotes strain hardening, as shown in Figure 13(a). However, due to the rapid movement of partial dislocations, the stacking faults are destroyed continuously, which increases the toughness.

In the later stage of deformation, 1/2 <110> perfect dislocations begin to move slowly and form plane slip bands. The strong interaction between perfect dislocations and partial dislocations hinders the rapid movement of partial dislocations, and the partial dislocations stop moving and begin to accumulate, resulting in strain hardening, as shown in Figure 13(b). In short, in the whole process of plastic deformation, the rapid movement of partial dislocation, the formation and disappearance of stacking fault parallelepiped, and the perfect dislocation/partial dislocation reaction make CrMnFeCoNi HEA both strong and tough.

Ding *et al.* [129] prepared a new CrFeCoNiPd high entropy, and *in situ* TEM strain test showed that its plastic deformation at room temperature mainly involved 1/2 <110> {111} perfect dislocation. At the initial stage of the deformation, the front end of the perfect dislocation is blocked by a strong obstacle, and the total dislocation moves slowly during the stacking process. As the movement of dislocations on the main slip surface is greatly resisted, many dislocations begin to cross slip, and a large number of cross slip dislocations are distributed almost everywhere. The cross slip of dislocations promotes the toughness of the HEA.

In the later stage of deformation, a large number of cross slip dislocations interact to promote strain hardening, and at the same time, secondary cross slip occurs.

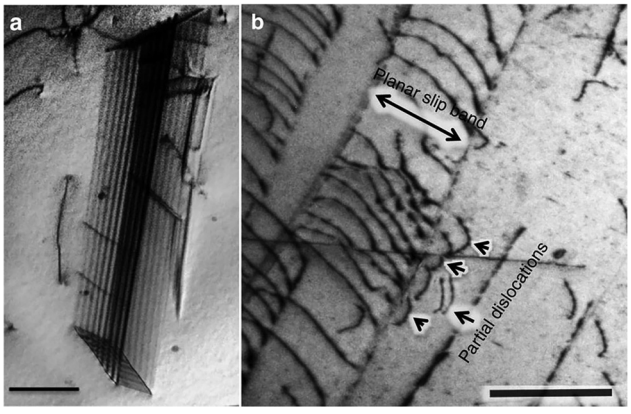


**Figure 13:** TEM of crack tip dislocation movement and stacking fault in the CrMnFeCoNi HEA, (a) the stacking fault parallelepiped, (b) dislocations with hindered movement [130].

Frequent cross slip and secondary cross slip promote toughness, while dislocation interaction promotes strain hardening, which is the reason for the strength and toughness of the CrFeCoNiPd HEA. Traditional plastic deformation mainly depends on perfect dislocation slip, partial dislocation slip, and twin deformation, while the CrFeCoNiPd HEA improves strength and toughness through uniformly distributed cross slip, which is a new plastic deformation method.

# 5 Critical appraisal of literature and outlook

The microstructure and mechanical properties of HEAs have been studied extensively, but there are still challenges in understanding the basic scientific problems and high-performance applications of HEAs. The current problems and future research directions of HEAs are summarized and prospected.

In terms of microstructure, the influence of composition effect on phase transformation remains in the shallow layer, and the cause of phase transformation has not been discussed fundamentally. High pressure-induced phase transition is mainly characterized by X-ray diffraction, which needs to be further characterized by more precise techniques, such as *in situ* high-pressure EXAFS. Besides, the establishment of phase diagram and thermodynamic model can help quantitatively analyze the relationship between microstructure and properties.

In terms of property, the mechanical properties of HEAs mainly focus on tension, compression, and hardness. Future research should strengthen the testing and analysis of fracture, wear, creep, and fatigue. In addition, according to the relevant theories of traditional alloys, the deformation mechanisms of HEAs are deduced, including dislocation movement, TWIP, and TRIP. However, the relationship between the deformation mechanism and the special lattice structure of high entropy solid solution has not been found.

In terms of strengthening mechanisms, the mechanisms of strengthening and toughening of HEAs are not deep enough. For example, HEAs can solve small atoms well, but the small atoms in the interstitial or lattice position have not been effectively proved. The details of TRIP effect and TWIP effect are still unclear. It can only be speculated that the TRIP effect produces volume expansion with the occurrence of martensitic transformation, which increases the range of uniform extension. The reason why TWIP effect can strengthen and toughen is

that the twin boundary hinders the movement of dislocations and allows dislocations to slide along the boundary, which improves strength and toughness. In addition, TRIP effect and TWIP effect are rarely applied to BCC HEAs (especially refractory HEAs) with high strength and poor toughness.

# 6 Summary

The emergence of HEAs provides a new choice for the design and research of high-performance metal materials. In this article, the preparation and forming mechanism, phase formation, phase transformation and strengthening, and toughening mechanism of HEAs are summarized as follows:

(1) The different preparation methods of HEAs were summarized and the corresponding forming mechanism was analyzed. The melting method and powder metallurgy were the most widely used in the preparation of HEAs.
(2) The factors affecting the formation of HEAs phase were summarized. Whether the HEAs can form solid solution phase can be deduced by calculating mixing entropy, mixing enthalpy, atomic size difference, and VEC.
(3) The inductive effects of elements, temperature, magnetism, and pressure on phase transition of HEAs were reviewed. The type and content of elements can affect the alloying behavior. Sintering or heat treatment can lead to the transformation of the metastable phase in HEAs. Magnetism affects the relative stability of FCC and HCP phases in HEAs. Stress induces phase transition by producing defects, strains, lattice distortion, changing magnetic state, and order degree.
(4) The strengthening and toughening mechanism of HEAs was discussed. The optimization effect of TRIP effect and TWIP effect on mechanical properties of HEAs was analyzed in detail. The relationship among concentration wave, dislocation motion, and mechanical properties of HEAs was analyzed.

**Funding information:** This work was supported by Key Laboratory of Infrared Imaging Materials and Detectors, Shanghai Institute of Technical Physics, Chinese Academy of Sciences (No. IIMDKFJJ-19-08) and China Postdoctoral Science Foundation (No. 2015M570794 and No. 2018T110993).

**Author contributions:** All authors have accepted responsibility for the entire content of this manuscript and approved its submission.

**Conflict of interest:** The authors state no conflict of interest.

# References

[1] Zhang H, Pan Y, He Y, Jiao H. Microstructure and properties of 6FeNiCoSiCrAlTi high-entropy alloy coating prepared by laser cladding. Appl Surf Sci. 2011;257(6):2259–63. doi: 10.1016/j.apsusc.2010.09.084.
[2] Yeh JW. Alloy design strategies and future trends in high-entropy alloys. Jom. 2013;65(12):1759–71. doi: 10.1007/s11837-013-0761-6.
[3] Senkov ON, Miller JD, Miracle DB, Woodward C. Accelerated exploration of multi-principal element alloys with solid solution phases. Nat Commun. 2015;6:6529–39. doi: 10.1038/ncomms7529.
[4] Chen LB, Wei R, Tang K, Zhang J, Jiang F, He L, et al. Heavy carbon alloyed FCC-structured high entropy alloy with excellent combination of strength and ductility. Mater Sci Eng A. 2018;716:150–6. doi: 10.1016/j.msea.2018.01.045.
[5] Zhang L, Huo X, Wang A, Du X, Zhang L, Li W, et al. A ductile high entropy alloy strengthened by nano sigma phase. Intermetallics. 2020;122:106813. doi: 10.1016/j.intermet.2020.106813.
[6] Lv S, Zu Y, Chen G, Zhao B, Fu X, Zhou W. A multiple non-metallic atoms co-doped CrMoNbWTi refractory high-entropy alloy with ultra-high strength and hardness. Mater Sci Eng A. 2020;795:140035. doi: 10.1016/j.msea.2020.140035.
[7] Zhu C, Li Z, Hong C, Dai P, Chen J. Microstructure and mechanical properties of the TiZrNbMoTa refractory high-entropy alloy produced by mechanical alloying and spark plasma sintering. Int J Refract Met Hard Mater. 2020;93:105357. doi: 10.1016/j.ijrmhm.2020.105357.
[8] Cao Y, Liu Y, Li Y, Liu B, Fu A, Nie Y. Precipitation behavior and mechanical properties of a hot-worked $TiNbTa_{0.5}ZrAl_{0.5}$ refractory high entropy alloy. Int J Refract Met Hard Mater. 2020;86:105132. doi: 10.1016/j.ijrmhm.2019.105132.
[9] Guo S, Liu CT. Phase stability in high entropy alloys: formation of solid-solution phase or amorphous phase. Prog Nat Sci Mater Int. 2011;21(6):433–46. doi: 10.1016/s1002-0071(12)60080-x.
[10] Guo S, Ng C, Lu J, Liu CT. Effect of valence electron concentration on stability of fcc or bcc phase in high entropy alloys. J Appl Phys. 2011;109(10):103505–42. doi: 10.1063/1.3587228.
[11] Lu W, Luo X, Yang Y, Huang B, Li P. Heterogeneous precipitates facilitate excellent mechanical properties in non-equiatomic medium-entropy alloy. Intermetallics. 2021;129:1–7. doi: 10.1016/j.intermet.2020.107036.
[12] Liang YJ, Wang L, Wen Y, Cheng B, Wu Q, Cao T, et al. High-content ductile coherent nanoprecipitates achieve

ultrastrong high-entropy alloys. Nat Commun. 2018;9(1):4063–74. doi: 10.1038/s41467-018-06600-8.
[13] Li Z, Pradeep KG, Deng Y, Raabe D, Tasan CC. Metastable high-entropy dual-phase alloys overcome the strength-ductility trade-off. Nature. 2016;534(7606):227–30. doi: 10.1038/nature17981.
[14] Li D, Li C, Feng T, Zhang Y, Sha G, Lewandowski JJ, et al. High-entropy $Al_{0.3}$CoCrFeNi alloy fibers with high tensile strength and ductility at ambient and cryogenic temperatures. Acta Mater. 2017;123:285–94. doi: 10.1016/j.actamat.2016.10.038.
[15] Liu WH, Lu ZP, He JY, Luan JH, Wang ZJ, Liu B, et al. Ductile CoCrFeNiMo$_x$ high entropy alloys strengthened by hard intermetallic phases. Acta Mater. 2016;116:332–42. doi: 10.1016/j.actamat.2016.06.063.
[16] Wang ZG, Zhou W, Fu LM, Wang JF, Luo RC, Han XC, et al. Effect of coherent L12 nanoprecipitates on the tensile behavior of a fcc-based high-entropy alloy. Mater Sci Eng A. 2017;696:503–10. doi: 10.1016/j.msea.2017.04.111.
[17] Yang T, Zhao YL, Luan JH, Han B, Wei J, Kai JJ, et al. Nanoparticles-strengthened high-entropy alloys for cryogenic applications showing an exceptional strength-ductility synergy. Scr Mater. 2019;164:30–5. doi: 10.1016/j.scriptamat.2019.01.034.
[18] Cheng B, Zhang F, Lou H, Chen X, Liaw PK, Yan J, et al. Pressure-induced phase transition in the AlCoCrFeNi high-entropy alloy. Scr Mater. 2019;161:88–92. doi: 10.1016/j.scriptamat.2018.10.020.
[19] George EP, Raabe D, Ritchie RO. High-entropy alloys. Nat Rev Mater. 2019;4(8):515–34. doi: 10.1038/s41578-019-0121-4.
[20] Nene SS, Frank M, Liu K, Mishra RS, McWilliams BA, Cho KC. Extremely high strength and work hardening ability in a metastable high entropy alloy. Sci Rep. 2018;8(1):9920–8. doi: 10.1038/s41598-018-28383-0.
[21] Wei D, Li X, Jiang J, Heng W, Koizumi Y, Choi WM, et al. Novel Co-rich high performance twinning-induced plasticity (TWIP) and transformation-induced plasticity (TRIP) high-entropy alloys. Scr Mater. 2019;165:39–43. doi: 10.1016/j.scriptamat.2019.02.018.
[22] Yeh JW, Chen SK, Lin SJ, Gan JY, Chin TS, Shun TT, et al. Nanostructured high-entropy alloys with multiple principal elements: Novel alloy design concepts and outcomes. Adv Eng Mater. 2004;6(5):299–303. doi: 10.1002/adem.200300567.
[23] Wang FJ, Zhang Y, Chen GL. Atomic packing efficiency and phase transition in a high entropy alloy. J Alloy Compd. 2009;478(1–2):321–4. doi: 10.1016/j.jallcom.2008.11.059.
[24] Tracy CL, Park S, Rittman DR, Zinkle SJ, Bei H, Lang M, et al. High pressure synthesis of a hexagonal close-packed phase of the high-entropy alloy CrMnFeCoNi. Nat Commun. 2017;8:15634–40. doi: 10.1038/ncomms15634.
[25] Niu C, LaRosa CR, Miao J, Mills MJ, Ghazisaeidi M. Magnetically-driven phase transformation strengthening in high entropy alloys. Nat Commun. 2018;9(1):1363–72. doi: 10.1038/s41467-018-03846-0.
[26] Ungricht EL, Culp C, Qu P, Harris JT, Brintz BJ, Mamalis N, et al. The effect of nanometer phase SiC addition on the microstructure and mechanical properties of $Al_{0.6}CrFe_2Ni_2$ high entropy alloys. Mater Technol. 2021;1–7. doi: 10.1080/10667857.2020.1863554.
[27] Yang S, Yan X, Yang K, Fu Z. Effect of the addition of nano-$Al_2O_3$ on the microstructure and mechanical properties of twinned $Al_{0.4}FeCrCoNi_{1.2}Ti_{0.3}$ alloys. Vacuum. 2016;131:69–72. doi: 10.1016/j.vacuum.2016.05.019.
[28] Zhang Y, Li J, Wang X, Lu Y, Zhou Y, Sun X. The interaction and migration of deformation twin in an eutectic high-entropy alloy AlCoCrFeNi$_{2.1}$. J Mate Sci Technol. 2019;35(5):902–6. doi: 10.1016/j.jmst.2018.09.067.
[29] Yang SF, Zhang Y, Yan X, Zhou H, Pi JH, Zhu DZ. Deformation twins and interface characteristics of nano-$Al_2O_3$ reinforced Al(0.4)AFeCrCo(1.5)NiTi(0.3) high entropy alloy composites. Mater Chem Phys. 2018;210:240–4. doi: 10.1016/j.matchemphys.2017.11.037.
[30] Sathiyamoorthi P, Kim HS. High-entropy alloys with heterogeneous microstructure: processing and mechanical properties. Prog Mater Sci. 2020;25:100709. doi: 10.1016/j.pmatsci.2020.100709.
[31] Li K, Chen W. Recent progress in high-entropy alloys for catalysts: synthesis, applications, and prospects. Mater Today Energy. 2021;20:100638. doi: 10.1016/j.mtener.2021.100638.
[32] Popescu G, Ghiban B, Popescu CA, Rosu L, Truscă R, Carcea I, et al. New TiZrNbTaFe high entropy alloy used for medical applications. IOP Conf Ser Mater Sci Eng. 2018;400(2):022049. doi: 10.1088/1757-899x/400/2/022049.
[33] Senkov ON, Senkova SV, Woodward C. Effect of aluminum on the microstructure and properties of two refractory high-entropy alloys. Acta Mater. 2014;68:214–28. doi: 10.1016/j.actamat.2014.01.029.
[34] Waseem OA, Lee J, Lee HM, Ryu HJ. The effect of Ti on the sintering and mechanical properties of refractory high-entropy alloy Ti$_x$WTaVCr fabricated *via* spark plasma sintering for fusion plasma-facing materials. Mater Chem Phys. 2018;210:87–94. doi: 10.1016/j.matchemphys.2017.06.054.
[35] Fu A, Guo W, Liu B, Cao Y, Xu L, Fang Q, et al. A particle reinforced NbTaTiV refractory high entropy alloy based composite with attractive mechanical properties. J Alloy Compd. 2020;815:152466. doi: 10.1016/j.jallcom.2019.152466.
[36] Jin G, Cai Z, Guan Y, Cui X, Liu Z, Li Y, et al. High temperature wear performance of laser-cladded FeNiCoAlCu high-entropy alloy coating. Appl Surf Sci. 2018;445:113–22. doi: 10.1016/j.apsusc.2018.03.135.
[37] Tian LH, Xiong W, Liu C, Lu S, Fu M. Microstructure and wear behavior of atmospheric plasma-sprayed AlCoCrFeNiTi high-entropy alloy coating. J Mater Eng Perform. 2016;25(12):5513–21. doi: 10.1007/s11665-016-2396-6.
[38] Anupam A, Kumar S, Chavan NM, Murty BS, Kottada RS. First report on cold-sprayed AlCoCrFeNi high-entropy alloy and its isothermal oxidation. J Mater Res. 2019;34(5):796–806. doi: 10.1557/jmr.2019.38.
[39] Liao W, Lan S, Gao L, Zhang H, Xu S, Song J, et al. Nanocrystalline high-entropy alloy (CoCrFeNiAl$_{0.3}$) thin-film coating by magnetron sputtering. Thin Solid Films. 2017;638:383–8. doi: 10.1016/j.tsf.2017.08.006.
[40] Xie L, Brault P, Bauchire J-M, Thomann A-L, Bedra L. Molecular dynamics simulations of clusters and thin film growth in the context of plasma sputtering deposition. J Phys

D. 2014;47(22):224004. doi: 10.1088/0022-3727/47/22/224004.
[41] Mileiko ST, Firstov SA, Novokhatskaya NA, Gorban VF, Krapivka NP. Oxide-fibre/high-entropy-alloy-matrix composites. Compos Part A Manuf. 2015;76:131–4. doi: 10.1016/j.compositesa.2015.05.023.
[42] Rekha MY, Mallik N, Srivastava C. First report on high entropy alloy nanoparticle decorated graphene. Sci Rep. 2018;8(1):8737–47. doi: 10.1038/s41598-018-27096-8.
[43] Li Z. Interstitial equiatomic CoCrFeMnNi high-entropy alloys: carbon content, microstructure, and compositional homogeneity effects on deformation behavior. Acta Mater. 2019;164:400–12. doi: 10.1016/j.actamat.2018.10.050.
[44] Deng Y, Tasan CC, Pradeep KG, Springer H, Kostka A, Raabe D. Design of a twinning-induced plasticity high entropy alloy. Acta Mater. 2015;94:124–33. doi: 10.1016/j.actamat.2015.04.014.
[45] He JY, Wang H, Huang HL, Xu XD, Chen MW, Wu Y, et al. A precipitation-hardened high-entropy alloy with outstanding tensile properties. Acta Mater. 2016;102:187–96. doi: 10.1016/j.actamat.2015.08.076.
[46] Fu Z, Jiang L, Wardini JL, MacDonald BE, Wen H, Xiong W, et al. A high-entropy alloy with hierarchical nanoprecipitates and ultrahigh strength. Sci Adv. 2018;4(10):8712–21. doi: 10.1126/sciadv.aat8712.
[47] Li T, Liu B, Liu Y, Guo W, Fu A, Li L, et al. Microstructure and mechanical properties of particulate reinforced NbMoCrTiAl high entropy based composite. Entropy. 2018;20(7):517–26. doi: 10.3390/e20070517.
[48] Fan QC, Li BS, Zhang Y. The microstructure and properties of (FeCrNiCo)AlCu high-entropy alloys and their TiC-reinforced composites. Mater Sci Eng A. 2014;598:244–50. doi: 10.1016/j.msea.2014.01.044.
[49] Yang S, Pi J, Yang W, Zhou H, Zhu D. Deformation twinning structure and interface in a FCC-based $Al_{0.3}FeNiCo_{1.2}$ CrCu high-entropy alloy matrix composites. Mater Lett. 2018;214:50–2. doi: 10.1016/j.matlet.2017.10.131.
[50] Torralba JM, Alvaredo P, García-Junceda A. High-entropy alloys fabricated *via* powder metallurgy. A critical review. Powder Metall. 2019;62(2):84–114. doi: 10.1080/00325899.2019.1584454.
[51] Xie Y, Cheng H, Tang Q, Chen W, Chen W, Dai P. Effects of N addition on microstructure and mechanical properties of CoCrFeNiMn high entropy alloy produced by mechanical alloying and vacuum hot pressing sintering. Intermetallics. 2018;93:228–34. doi: 10.1016/j.intermet.2017.09.013.
[52] Yang D, Liu Y, Jiang H, Liao M, Qu N, Han T, et al. A novel FeCrNiAlTi-based high entropy alloy strengthened by refined grains. J Alloy Compd. 2020;823:153729. doi: 10.1016/j.jallcom.2020.153729.
[53] Sharma A, Oh MC, Ahn B. Microstructural evolution and mechanical properties of non-Cantor AlCuSiZnFe lightweight high entropy alloy processed by advanced powder metallurgy. Mater Sci Eng A. 2020;797:140066. doi: 10.1016/j.msea.2020.140066.
[54] Fu Z, Chen W, Wen H, Zhang D, Chen Z, Zheng B, et al. Microstructure and strengthening mechanisms in an FCC structured single-phase nanocrystalline $Co_{25}Ni_{25}Fe2_5Al_{7.5}Cu_{17.5}$ high-entropy alloy. Acta Mater. 2016;107:59–71. doi: 10.1016/j.actamat.2016.01.050.
[55] Zhang H, Pan Y, He YZ. Synthesis and characterization of FeCoNiCrCu high-entropy alloy coating by laser cladding. Mater Des. 2011;32(4):1910–5. doi: 10.1016/j.matdes.2010.12.001.
[56] Mu YK, Jia YD, Xu L, Jia YF, Tan XH, Yi J, et al. Nano oxides reinforced high-entropy alloy coatings synthesized by atmospheric plasma spraying. Mater Res Lett. 2019;7(8):312–9. doi: 10.1080/21663831.2019.1604443.
[57] Liu X-T, Lei W-B, Li J, Ma Y, Wang W-M, Zhang B-H, et al. Laser cladding of high-entropy alloy on H13 steel. Rare Met. 2014;33(6):727–30. doi: 10.1007/s12598-014-0403-3.
[58] Braeckman BR, Depla D. Structure formation and properties of sputter deposited Nbx-CoCrCuFeNi high entropy alloy thin films. J Alloy Compd. 2015;646:810–5. doi: 10.1016/j.jallcom.2015.06.097.
[59] Liu WH, Wu Y, He JY, Nieh TG, Lu ZP. Grain growth and the Hall–Petch relationship in a high-entropy FeCrNiCoMn alloy. Scr Mater. 2013;68(7):526–9. doi: 10.1016/j.scriptamat.2012.12.002.
[60] Li Z, Tasan CC, Pradeep KG, Raabe D. A TRIP-assisted dual-phase high-entropy alloy: grain size and phase fraction effects on deformation behavior. Acta Mater. 2017;131:323–35. doi: 10.1016/j.actamat.2017.03.069.
[61] Sathiyamoorthi P, Basu J, Kashyap S, Pradeep KG, Kottada RS. Thermal stability and grain boundary strengthening in ultrafine-grained CoCrFeNi high entropy alloy composite. Mater Des. 2017;134:426–33. doi: 10.1016/j.matdes.2017.08.053.
[62] Ganji RS, Sai Karthik P, Bhanu Sankara Rao K, Rajulapati KV. Strengthening mechanisms in equiatomic ultrafine grained AlCoCrCuFeNi high-entropy alloy studied by micro- and nanoindentation methods. Acta Mater. 2017;125:58–68. doi: 10.1016/j.actamat.2016.11.046.
[63] Long Y, Liang X, Su K, Peng H, Li X. A fine-grained NbMoTaWVCr refractory high-entropy alloy with ultra-high strength: microstructural evolution and mechanical properties. J Alloy Compd. 2019;780:607–17. doi: 10.1016/j.jallcom.2018.11.318.
[64] Wang J, Kuang S, Yu X, Wang L, Huang W. Tribo-mechanical properties of CrNbTiMoZr high-entropy alloy film synthesized by direct current magnetron sputtering. Surf Coat Technol. 2020;403:126374. doi: 10.1016/j.surfcoat.2020.126374.
[65] Chawake N, Zálešák J, Gammer C, Franz R, Cordill MJ, Kim JT, et al. Microstructural characterization of medium entropy alloy thin films. Scr Mater. 2020;177:22–6. doi: 10.1016/j.scriptamat.2019.10.001.
[66] Yim D, Sathiyamoorthi P, Hong S-J, Kim HS. Fabrication and mechanical properties of TiC reinforced CoCrFeMnNi high-entropy alloy composite by water atomization and spark plasma sintering. J Alloy Compd. 2019;781:389–96. doi: 10.1016/j.jallcom.2018.12.119.
[67] Liu X, Zhang L, Xu Y. Microstructure and mechanical properties of graphene reinforced $Fe_{50}Mn_{30}Co_{10}Cr_{10}$ high-entropy alloy composites synthesized by MA and SPS. Appl Phys A. 2017;123(9):567–74. doi: 10.1007/s00339-017-1151-7.
[68] Gao X, Yue H, Guo E, Zhang H, Lin X, Yao L, et al. Preparation and tensile properties of homogeneously dispersed graphene reinforced aluminum matrix composites. Mater Des. 2016;94:54–60. doi: 10.1016/j.matdes.2016.01.034.

[69] Singh S, Shaikh SM, Kumar MKP, Murty BS, Srivastava C. Microstructural homogenization and substantial improvement in corrosion resistance of mechanically alloyed FeCoCrNiCu high entropy alloys by incorporation of carbon nanotubes. Materialia. 2020;14:100917. doi: 10.1016/j.mtla.2020.100917.

[70] Sun X, Zhu H, Li J, Huang J, Xie Z. High entropy alloy FeCoNiCu matrix composites reinforced with *in situ* TiC particles and graphite whiskers. Mater Chem Phys. 2018;220:449–59. doi: 10.1016/j.matchemphys.2018.09.022.

[71] Sun X, Zhu H, Li J, Huang J, Xie Z. Influence of aluminum content on the microstructure and properties of the *in situ* TiC reinforced $Al_x$FeCoNiCu high entropy alloy matrix composites. Mater Sci Eng A. 2019;743:540–5. doi: 10.1016/j.msea.2018.11.120.

[72] Wang Z, Huang Y, Yang Y, Wang J, Liu CT. Atomic-size effect and solid solubility of multicomponent alloys. Scr Mater. 2015;94:28–31. doi: 10.1016/j.scriptamat.2014.09.010.

[73] Miracle DB, Senkov ON. A critical review of high entropy alloys and related concepts. Acta Mater. 2017;122:448–511. doi: 10.1016/j.actamat.2016.08.081.

[74] Yang X, Zhang Y. Prediction of high-entropy stabilized solid-solution in multi-component alloys. Mater Chem Phys. 2012;132(2–3):233–8. doi: 10.1016/j.matchemphys.2011.11.021.

[75] Chen H, Kauffmann A, Gorr B, Schliephake D, Seemüller C, Wagner JN, et al. Microstructure and mechanical properties at elevated temperatures of a new Al-containing refractory high-entropy alloy Nb-Mo-Cr-Ti-Al. J Alloy Compd. 2016;661:206–15. doi: 10.1016/j.jallcom.2015.11.050.

[76] Alaneme KK, Bodunrin MO, Oke SR. Processing, alloy composition and phase transition effect on the mechanical and corrosion properties of high entropy alloys: a review. J Mater Res Technol. 2016;5(4):384–93. doi: 10.1016/j.jmrt.2016.03.004.

[77] Guo S, Hu Q, Ng C, Liu CT. More than entropy in high-entropy alloys: forming solid solutions or amorphous phase. Intermetallics. 2013;41:96–103. doi: 10.1016/j.intermet.2013.05.002.

[78] Wu Y, Zhang F, Yuan X, Huang H, Wen X, Wang Y, et al. Short-range ordering and its effects on mechanical properties of high-entropy alloys. J Mater Sci Technol. 2021;62:214–20. doi: 10.1016/j.jmst.2020.06.018.

[79] Zhao K, Xia XX, Bai HY, Zhao DQ, Wang WH. Room temperature homogeneous flow in a bulk metallic glass with low glass transition temperature. Appl Phys Lett. 2011;98(14):141913–42. doi: 10.1063/1.3575562.

[80] Cunliffe A, Plummer J, Figueroa I, Todd I. Glass formation in a high entropy alloy system by design. Intermetallics. 2012;23:204–7. doi: 10.1016/j.intermet.2011.12.006.

[81] Tsai MH, Yeh JW. High-entropy alloys: a critical review. Mater Res Lett. 2014;2(3):107–23. doi: 10.1080/21663831.2014.912690.

[82] Ye YF, Liu CT, Yang Y. A geometric model for intrinsic residual strain and phase stability in high entropy alloys. Acta Mater. 2015;94:152–61. doi: 10.1016/j.actamat.2015.04.051.

[83] Chen W, Fu Z, Fang S, Xiao H, Zhu D. Alloying behavior, microstructure and mechanical properties in a $FeNiCrCo_{0.3}Al_{0.7}$ high entropy alloy. Mater Des. 2013;51:854–60. doi: 10.1016/j.matdes.2013.04.061.

[84] Ferrari V, Wolf W, Zepon G, Coury FG, Kaufman MJ, Bolfarini C, et al. Effect of boron addition on the solidification sequence and microstructure of AlCoCrFeNi alloys. J Alloy Compd. 2019;775:1235–43. doi: 10.1016/j.jallcom.2018.10.268.

[85] Varalakshmi S, Kamaraj M, Murty BS. Processing and properties of nanocrystalline CuNiCoZnAlTi high entropy alloys by mechanical alloying. Mater Sci Eng A. 2010;527(4–5):1027–30. doi: 10.1016/j.msea.2009.09.019.

[86] He JY, Liu WH, Wang H, Wu Y, Liu XJ, Nieh TG, et al. Effects of Al addition on structural evolution and tensile properties of the FeCoNiCrMn high-entropy alloy system. Acta Mater. 2014;62:105–13. doi: 10.1016/j.actamat.2013.09.037.

[87] Ji W, Fu Z, Wang W, Wang H, Zhang J, Wang Y, et al. Mechanical alloying synthesis and spark plasma sintering consolidation of CoCrFeNiAl high-entropy alloy. J Alloy Compd. 2014;589:61–6. doi: 10.1016/j.jallcom.2013.11.146.

[88] Ji W, Wang W, Wang H, Zhang J, Wang Y, Zhang F, et al. Alloying behavior and novel properties of CoCrFeNiMn high-entropy alloy fabricated by mechanical alloying and spark plasma sintering. Intermetallics. 2015;56:24–7. doi: 10.1016/j.intermet.2014.08.008.

[89] Chen LB, Wei R, Tang K, Zhang J, Jiang F, Sun J. Ductile-brittle transition of carbon alloyed $Fe_{40}Mn_{40}Co_{10}Cr_{10}$ high entropy alloys. Mater Lett. 2019;236:416–9. doi: 10.1016/j.matlet.2018.10.144.

[90] Zhang F, Wu Y, Lou H, Zeng Z, Prakapenka VB, Greenberg E, et al. Polymorphism in a high-entropy alloy. Nat Commun. 2017;8:15687. doi: 10.1038/ncomms15687.

[91] Chen L, Bobzin K, Zhou Z, Zhao L, Öte M, Königstein T, et al. Effect of heat treatment on the phase composition, microstructure and mechanical properties of $Al_{0.6}$CrFeCoNi and $Al_{0.6}$CrFeCoNi$Si_{0.3}$ high-entropy alloys. Metals. 2018;8(11):974–87. doi: 10.3390/met8110974.

[92] Ma D, Grabowski B, Körmann F, Neugebauer J, Raabe D. *Ab initio* thermodynamics of the CoCrFeMnNi high entropy alloy: importance of entropy contributions beyond the configurational one. Acta Mater. 2015;100:90–7. doi: 10.1016/j.actamat.2015.08.050.

[93] Miller A, Carchman R, Long R, Denslow SA. Pressure-induced fcc to hcp phase transition in Ni-based high entropy solid solution alloys. Appl Phys Lett. 2017;110(1):011902–42. doi: 10.1063/1.4973627.

[94] Miller A, Carchman R, Long R, Denslow SA. Structural stability of high entropy alloys under pressure and temperature. J Appl Phys. 2017;121(23):235901–42. doi: 10.1063/1.4984796.

[95] Guo J, Wang H, von Rohr F, Wang Z, Cai S, Zhou Y, et al. Robust zero resistance in a superconducting high-entropy alloy at pressures up to 190 GPa. Proc Natl Acad Sci USA. 2017;114(50):13144–7. doi: 10.1073/pnas.1716981114.

[96] Torchio R, Mathon O, Pascarelli S. XAS and XMCD spectroscopies to study matter at high pressure: probing the correlation between structure and magnetism in the 3d metals. Coord Chem Rev. 2014;277–278:80–94. doi: 10.1016/j.ccr.2014.02.024.

[97] Liu KC, Gupta D. Pressure-induced magnetovolume effect in CoCrFeAl high-entropy alloy. Commun Phys. 2019;2(1):166. doi: 10.1038/s42005-019-0141-9.

[98] Tian F, Varga LK, Shen J, Vitos L. Calculating elastic constants in high-entropy alloys using the coherent potential

approximation: current issues and errors. Comput Mater Sci. 2016;111:350–8. doi: 10.1016/j.commatsci.2015.09.058.
[99] Ma Y, Fan J, Zhang L, Zhang M, Cui P, Dong W, et al. Pressure-induced ordering phase transition in high-entropy alloy. Intermetallics. 2018;103:63–6. doi: 10.1016/j.intermet.2018.10.003.
[100] Zhang FX, Zhao S, Jin K, Xue H, Velisa G, Bei H, et al. Local structure and short-range order in a NiCoCr solid solution alloy. Phys Rev Lett. 2017;118(20):205501. doi: 10.1103/PhysRevLett.118.205501.
[101] Wei Q, Shen Q, Zhang J, Chen B, Luo G, Zhang L. Microstructure and mechanical property of a novel ReMoTaW high-entropy alloy with high density. Int J Refract Met Hard Mater. 2018;77:8–11. doi: 10.1016/j.ijrmhm.2018.05.006.
[102] Juan CC, Tseng KK, Hsu WL, Tsai MH, Tsai CW, Lin CM, et al. Solution strengthening of ductile refractory $HfMo_xNbTaTiZr$ high-entropy alloys. Mater Lett. 2016;175:284–7. doi: 10.1016/j.matlet.2016.03.133.
[103] Han SK, Wu MF, Cui S, Wagner D. Phase composition and solid solution strengthening effect in TiZrNbMoV high-entropy alloys. Mater Des. 2015;83:651–60. doi: 10.1016/j.matdes.2015.06.072.
[104] Senkov ON, Scott JM, Senkova SV, Miracle DB, Woodward CF. Microstructure and room temperature properties of a high-entropy TaNbHfZrTi alloy. J Alloy Compd. 2011;509(20):6043–8. doi: 10.1016/j.jallcom.2011.02.171.
[105] Wang Z, Baker I, Cai Z, Chen S, Poplawsky JD, Guo W. The effect of interstitial carbon on the mechanical properties and dislocation substructure evolution in $Fe_{40.4}Ni_{11.3}Mn_{34.8}Al_{7.5}Cr_6$ high entropy alloys. Acta Mater. 2016;120:228–39. doi: 10.1016/j.actamat.2016.08.072.
[106] Zhao ZY, Guan RG, Guan XH, Feng ZX, Chen H, Chen Y. Microstructures and properties of graphene-Cu/Al composite prepared by a novel process through clad forming and improving wettability with copper. Adv Eng Mater. 2015;17(5):663–8. doi: 10.1002/adem.201400173.
[107] Chen Y, Zhang X, Liu E, He C, Shi C, Li J, et al. Fabrication of *in situ* grown graphene reinforced Cu matrix composites. Sci Rep. 2016;6:19363. doi: 10.1038/srep19363.
[108] Rogal Ł, Kalita D, Tarasek A, Bobrowski P, Czerwinski F. Effect of SiC nano-particles on microstructure and mechanical properties of the CoCrFeMnNi high entropy alloy. J Alloy Compd. 2017;708:344–52. doi: 10.1016/j.jallcom.2017.02.274.
[109] Wu H, Huang S, Qiu H, Zhu H, Xie Z. Effect of Si and C additions on the reaction mechanism and mechanical properties of FeCrNiCu high entropy alloy. Sci Rep. 2019;9(1):16356. doi: 10.1038/s41598-019-52809-y.
[110] Chen S, Oh HS, Gludovatz B, Kim SJ, Park ES, Zhang Z et al. Real-time observations of TRIP-induced ultrahigh strain hardening in a dual-phase CrMnFeCoNi high-entropy alloy. Nat Commun. 2020;11(1):826–34. doi: 10.1038/s41467-020-14641-1.
[111] Lu W, Liebscher CH, Dehm G, Raabe D, Li Z. Bidirectional transformation enables hierarchical nanolaminate dual-phase high-entropy alloys. Adv Mater. 2018;30(44):1804727. doi: 10.1002/adma.201804727s.
[112] Fang Q, Chen Y, Li J, Jiang C, Liu B, Liu Y, et al. Probing the phase transformation and dislocation evolution in dual-phase high-entropy alloys. Int J Plast. 2019;114:161–73. doi: 10.1016/j.ijplas.2018.10.014.
[113] Li X, Irving DL, Vitos L. First-principles investigation of the micromechanical properties of fcc-hcp polymorphic high-entropy alloys. Sci Rep. 2018;8(1):11196. doi: 10.1038/s41598-018-29588-z.
[114] Liu SF, Wu Y, Wang HT, Lin WT, Shang YY, Liu JB, et al. Transformation-reinforced high-entropy alloys with superior mechanical properties *via* tailoring stacking fault energy. J Alloy Compd. 2019;792:444–55. doi: 10.1016/j.jallcom.2019.04.035.
[115] Nene SS, Liu K, Frank M, Mishra RS, Brennan RE, Cho KC, et al. Enhanced strength and ductility in a friction stir processing engineered dual phase high entropy alloy. Sci Rep. 2017;7(1):16167. doi: 10.1038/s41598-017-16509-9.
[116] Guimarães JRC, Rios PR. Martensite start temperature and the austenite grain-size. J Mater Sci. 2010;45(4):1074–7. doi: 10.1007/s10853-009-4044-0.
[117] Pisarik ST, Van Aken DC. Thermodynamic driving force of the $\gamma \rightarrow \varepsilon$ transformation and resulting MS temperature in high-Mn steels. Metall Mater Trans A. 2015;47(3):1009–18. doi: 10.1007/s11661-015-3265-x.
[118] Li W, Liaw PK, Gao Y. Fracture resistance of high entropy alloys: a review. Intermetallics. 2018;99:69–83. doi: 10.1016/j.intermet.2018.05.013.
[119] Zhang Y, Zuo TT, Tang Z, Gao MC, Dahmen KA, Liaw PK, et al. Microstructures and properties of high-entropy alloys. Prog Mater Sci. 2014;61:1–93. doi: 10.1016/j.pmatsci.2013.10.001.
[120] Gludovatz B, Hohenwarter A, Catoor D, Chang EH, George EP, Ritchie RO. A fracture-resistant high-entropy alloy for cryogenic applications. Science. 2014;345(6201):1153–8. doi: 10.1126/science.1254581.
[121] Zhang Y, Li J, Wang J, Wang WY, Kou H, Beaugnon E. Temperature dependent deformation mechanisms of $Al_{0.3}$CoCrFeNi high-entropy alloy, starting from serrated flow behavior. J Alloy Compd. 2018;757:39–43. doi: 10.1016/j.jallcom.2018.04.305.
[122] Chen B, Li S, Imai H, Jia L, Umeda J, Takahashi M, et al. Load transfer strengthening in carbon nanotubes reinforced metal matrix composites *via in situ* tensile tests. Compos Sci Technol. 2015;113:1–8. doi: 10.1016/j.compscitech.2015.03.009.
[123] Fu Z, Koc R. Ultrafine $TiB_2$-TiNiFeCrCoAl high-entropy alloy composite with enhanced mechanical properties. Mater Sci Eng A. 2017;702:184–8. doi: 10.1016/j.msea.2017.07.008.
[124] Luo W, Liu Y, Shen J. Effects of binders on the microstructures and mechanical properties of ultrafine WC-10% $Al_x$CoCrCuFeNi composites by spark plasma sintering. J Alloy Compd. 2019;791:540–9. doi: 10.1016/j.jallcom.2019.03.328.
[125] Kim SW, Kim JH. *In situ* observations of deformation twins and crack propagation in a CoCrFeNiMn high-entropy alloy. Mater Sci Eng A. 2018;718:321–5. doi: 10.1016/j.msea.2018.01.121.
[126] Ming K, Bi X, Wang J. Microstructures and deformation mechanisms of $Cr_{26}Mn_{20}Fe_{20}Co_{20}Ni_{14}$ alloys. Mater Charact. 2017;134:194–201. doi: 10.1016/j.matchar.2017.10.022.

[127] Ghassemali E, Sonkusare R, Biswas K, Gurao NP. *In situ* study of crack initiation and propagation in a dual phase AlCoCrFeNi high entropy alloy. J Alloy Compd. 2017;710:539–46. doi: 10.1016/j.jallcom.2017.03.307.

[128] Li QJ, Sheng H, Ma E. Strengthening in multi-principal element alloys with local-chemical-order roughened dislocation pathways. Nat Commun. 2019;10(1):3563–74. doi: 10.1038/s41467-019-11464-7.

[129] Ding Q, Zhang Y, Chen X, Fu X, Chen D, Chen S, et al. Tuning element distribution, structure and properties by composition in high-entropy alloys. Nature. 2019;574(7777):223–7. doi: 10.1038/s41586-019-1617-1.

[130] Zhang Z, Mao MM, Wang J, Gludovatz B, Zhang Z, Mao SX, et al. Nanoscale origins of the damage tolerance of the high-entropy alloy CrMnFeCoNi. Nat Commun. 2015;6:10143. doi: 10.1038/ncomms10143.